An OVERVIEW of Research and Development Activities in Machine Design and Drives

Prof. B. G. Fernandes

IIT Bombay

Flux Reversal Machine (FRM) for Rooftop Wind Energy Conversion

- Both windings and PMs are on stator
- Rotor has salient structure and no PMs or windings
- Rotor is simple and robust
- Conventional FRM → low winding factor of 0.5 due to concentrated winding
- Designed FRM → full pitch winding
  Improves winding factor to 1
- Prototype specs:
  - 6 stator poles with 4 magnets/pole
  - 14 rotor poles
  - 214 rpm, 50 Hz, 90 V, 20 A

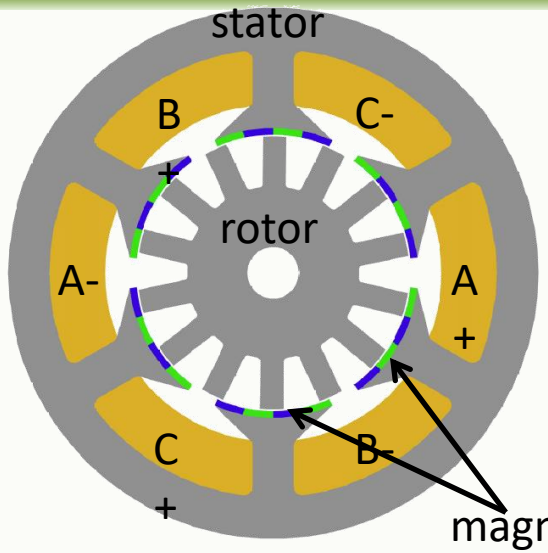

FRM geometry

Stator

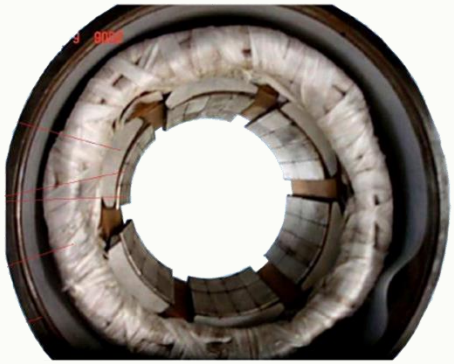

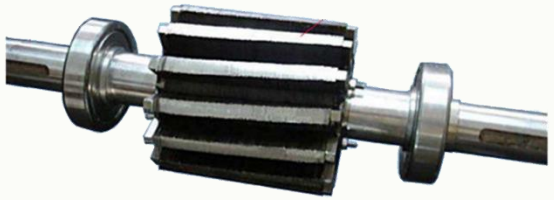

Rotor

Prototype of FRM

[1] D. S. More and B. G. Fernandes, "Modeling and Performance of Three Phase 6/14 Pole Flux Reversal Machine," IET Electric Power Applications, vol. 7, no. 2, pp. 131-139, Feb. 2013.

Slotless Permanent Magnet Generator for Wind Power Conversion

- Axial flux PM topology → high energy density
- Slot-less stator → no spiral laminations on stator
  → low cost
- Dual rotor single stator with toroidal winding
  → lower copper loss
- Low speed design with 16 rotor poles
  → direct coupling with wind turbine
- Gear box is eliminated
  → high efficiency, lower cost
- Prototype specifications:

Power	1 kW
Voltage	230 V
Rotor poles	16

Stator

The two rotors

High Torque Density Axial Flux PM Motor for Elevator Application

- Elevators require high torque, low speed motor
- Axial flux PM motor
  → better utilization of available space
- Low speed motor → high number of rotor poles
  → improves specific torque
- Skewed stator slots → reduced cogging torque

Stator

- Prototype specifications:

Power	12 kW @ 150 rpm
Torque	764 Nm
Slots / poles	72/24
Outer diameter	800 mm
Axial length	220 mm
Estimated efficiency	92%

Rotor

High Speed Axial Flux Motor for Flywheel Energy Storage

- Axial flux topology → high energy density
- PM based motor → high efficiency (PMs: SmCo)
- High speed rotor: 24000 rpm
- Steel used: 40Ni2Cr1Mo28 → high rotor strength
- Dual stator, single rotor design
- Prototype specifications:

Power	4 kW @ 24,000 rpm
Stator slots	24
Rotor poles	8
Frequency	800 Hz
Copper loss	24 W
Iron loss	264 W
Efficiency	81 %

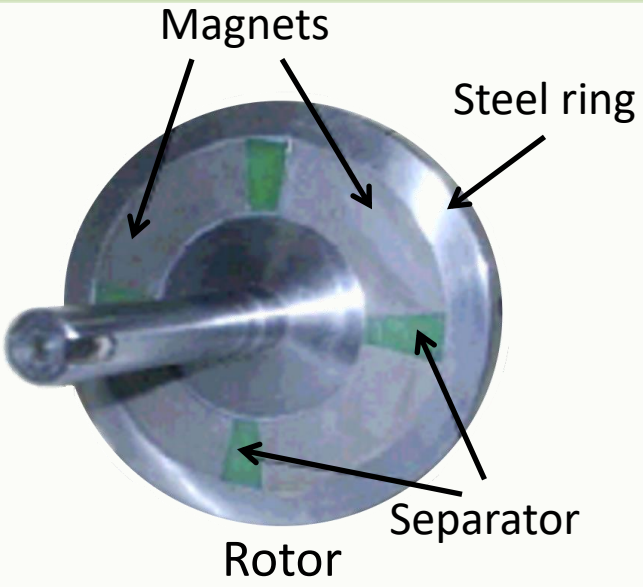

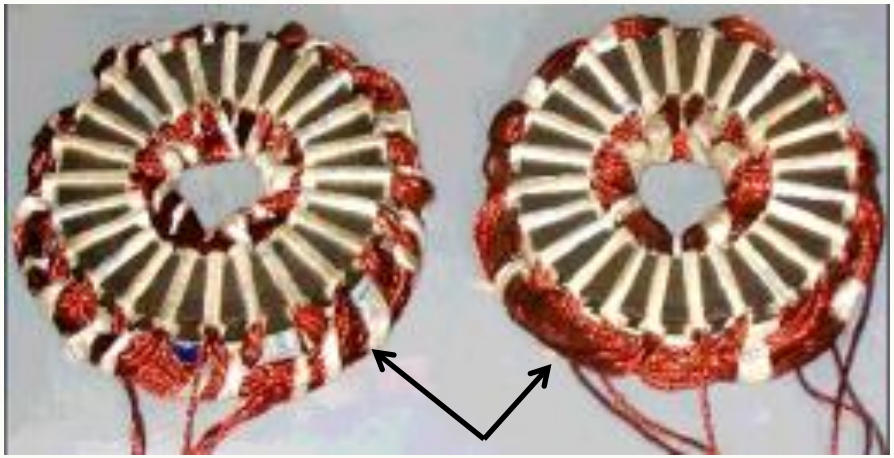

The two stators

High Speed Axial Flux Motor for Centrifuge Application

- Axial flux topology → high speed application
- PM based motor→ high efficiency (PMs: SmCo)
- High speed rotor: 45,000 rpm, slotless stator
- Single stator, single rotor → should be able to run continuously for 20 years

- Prototype specifications

Power	94 W @ 45,000 rpm
Stator slots	12
Rotor poles	4
Outer diameter	140 mm
Length	50 mm
Efficiency	> 65 %

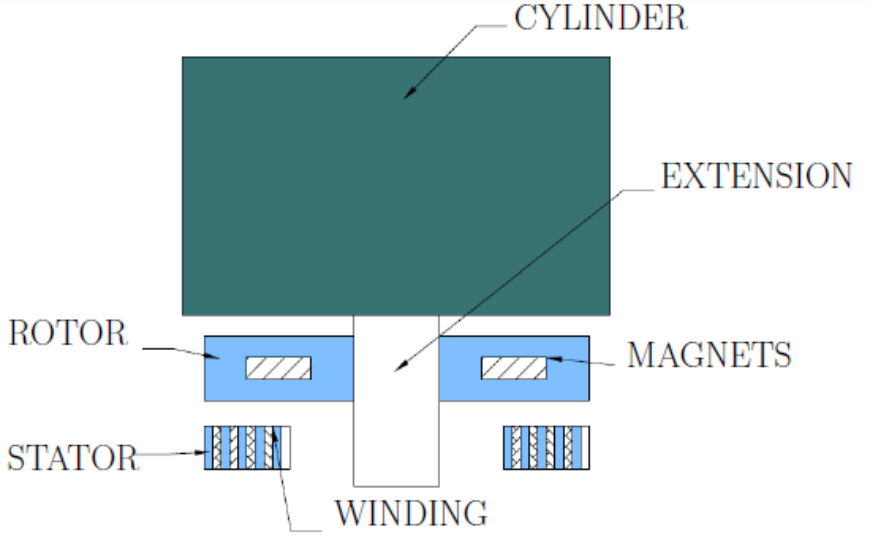

Fig. Cross-section view of Axial flux motor

High Speed Axial Flux Motor for Centrifuge Application

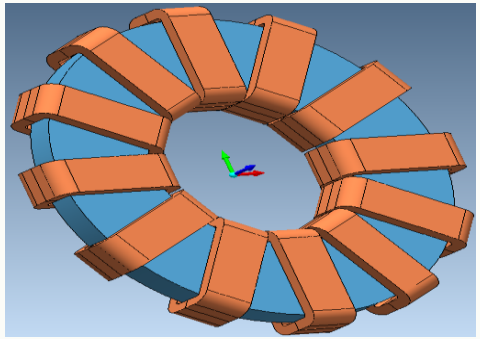

(a)

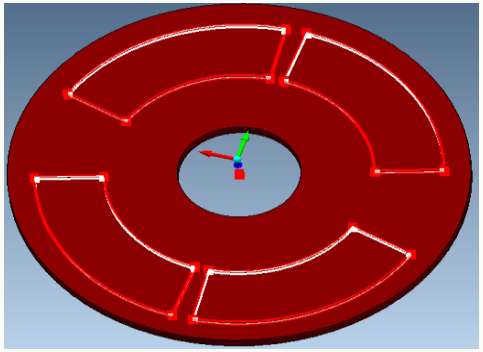

(b)

(c)

Fig. FEM models of the (a) stator and (b) rotor of the axial flux motor with magnetic core;
(c) Experimental prototype and (d) Voltage and current waveforms measured at 20,000 rpm

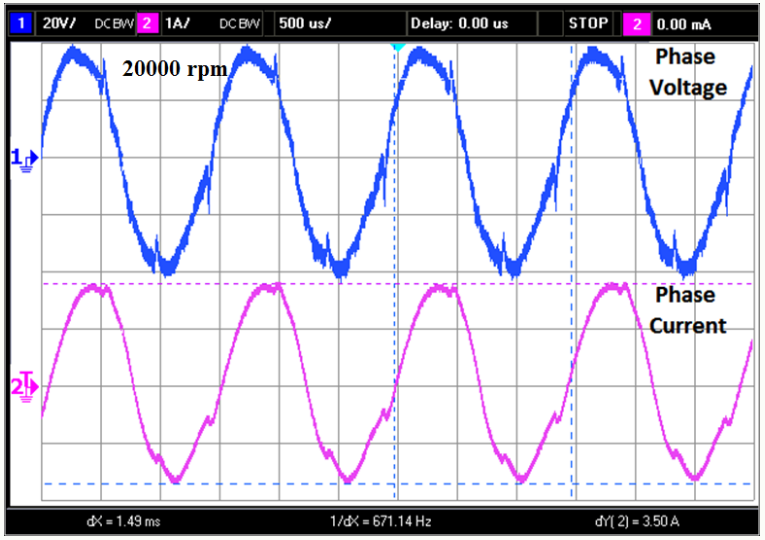

(d)

[1] S. Neethu, S. Pal, A. K. Wankhede and B. G. Fernandes, "High performance axial flux permanent magnet synchronous motor for high speed applications," *IECON 2017*, Beijing, 2017, pp. 5093-5098.

Coreless Axial Flux Permanent Magnet Motor with PCB Winding

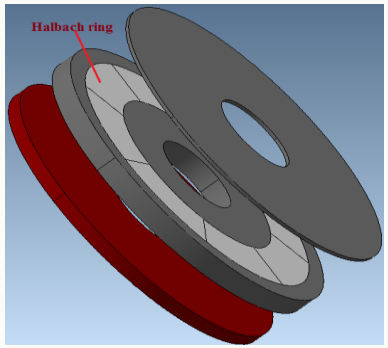

(a)

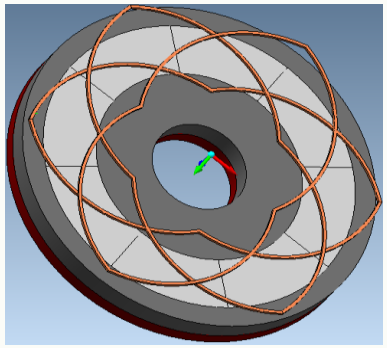

(b)

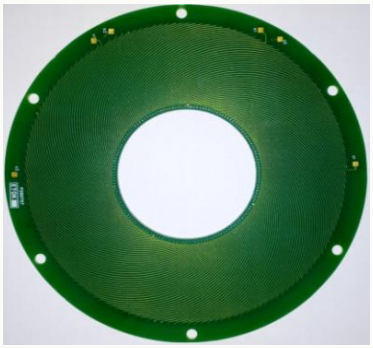

(c)

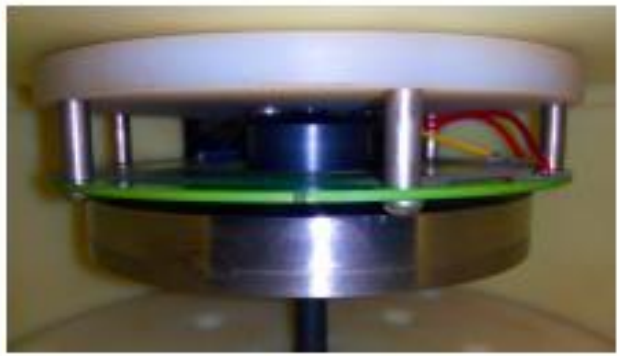

(d)

Fig. Coreless axial flux permanent magnet (AFPM) motor (a) Exploded view of the Halbach rotor arrangement, and (b) Basic layout of the PCB winding; Experimental prototype of AFPM (c) Multilayer PCB stator, (d) Motor assembly and (e) Recorded waveforms at 24,000 rpm[1]

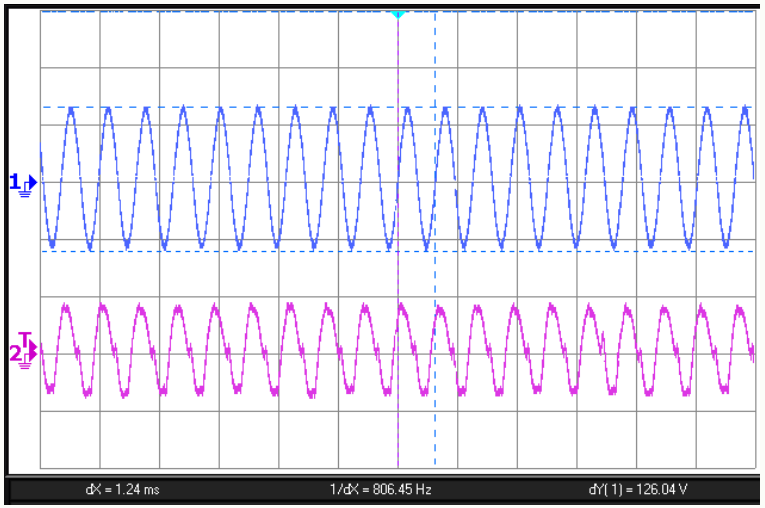

(e)

---

[1] N. S., S. P. Nikam, S. Singh, S. Pal, A. K. Wankhede and B. G. Fernandes, "High-Speed Coreless Axial Flux Permanent Magnet Motor with Printed Circuit Board Winding," in IEEE Transactions on Industry Applications.

Line-start Permanent Magnet Synchronous Motor for Irrigation Pumps

- Permanent magnet motor → higher efficiency
- Buried PMs are used with a squirrel cage for line start capability
- Line start capability → eliminates PE inverter → low cost

- Novel rotor geometry:
  - High flux concentration:
    → low cost ferrites can be used
  - High efficiency and specific power
  - Can synchronize at lower voltage
  - High power factor : 0.97

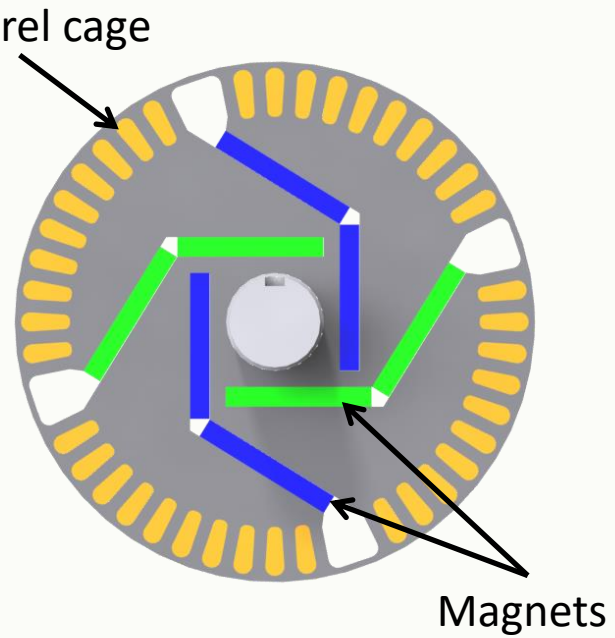

Rotor geometry

Line-Start Ferrite Assisted Synchronous Reluctance Motor for Bore-Well Pump

- This particular motor design offers high rotor saliency.
- Rotor cage is embedded in the reluctance path of the flux barriers to obtain improved starting characteristic and rotor synchronization.
- Improved motor efficiency is achieved, which meets the new international efficiency (IE-4) standard for line-start application.[1]

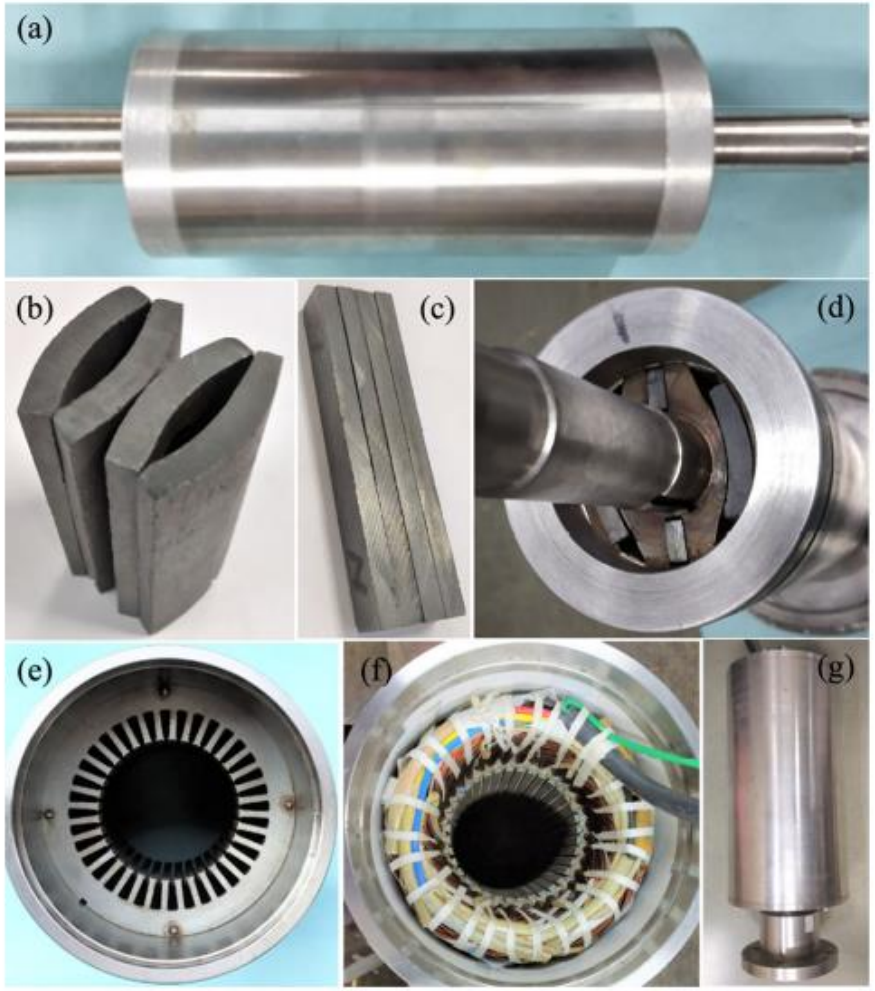

Fig. Prototype of the ferrite assisted LS SyRM (a) finished rotor, (b)-(c) arc and rectangular ferrite magnets, (d) magnets placed in the rotor, (e) stator inside the frame, (f) star-connected distributed winding on the stator and (g) assembled motor.[1]

[1] S. Baka, S. Sashidhar and B. G. Fernandes, "Design and Optimization of a Two-Pole Line-Start Ferrite Assisted Synchronous Reluctance Motor," ICEM 2018, Alexandroupoli, Greece, 2018, pp. 131-137.

Toroidal Winding for Efficiency Improvement of a 5 hp Induction Machine

- Salient features of the Toroidal winding SCIM[1]
  - Wound around the stator back-iron.
  - High stator fill-factor (≈ 0.6).
  - Non-overlapping coils.
  - Simple coil winding leads to ease of manufacturing.
  - Aluminum is used as the rotor bar material.
- Conclusion: Toroidal winding helps improve efficiency in squirrel cage induction machine (SCIM).

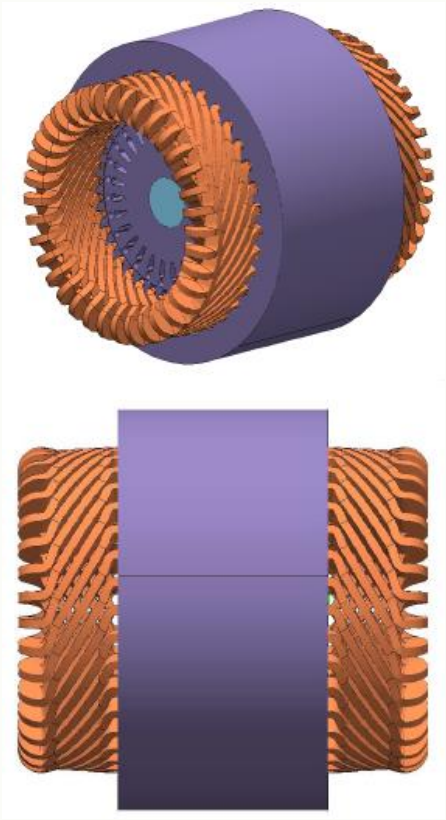

(a)

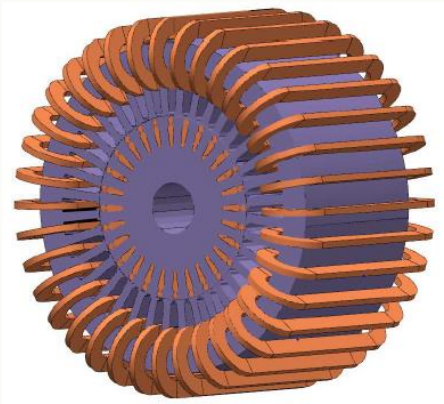

(b)

Fig. Comparative study between SCIM models with (a) distributed and (b) toroidal windings[1].

[1] S. Sashidhar, S. Mathew and B. G. Fernandes, "Novel Toroidal Winding for Efficiency Improvement of a Line-Start Induction Motor," *IECON 2018*, pp. 607-612, doi: 10.1109/IECON.2018.8591812.

Low-Cost High Speed BLDC motor for PV Based Deep Bore-well Submersible Pump

Problem:

- Motor has to fit inside a 4-inch bore-well (100 mm) & should be submersible.
- Motor has to be tubular (< D/L ratio).
- High current density
- High speed pump (2880 rpm, 2 H.P.)

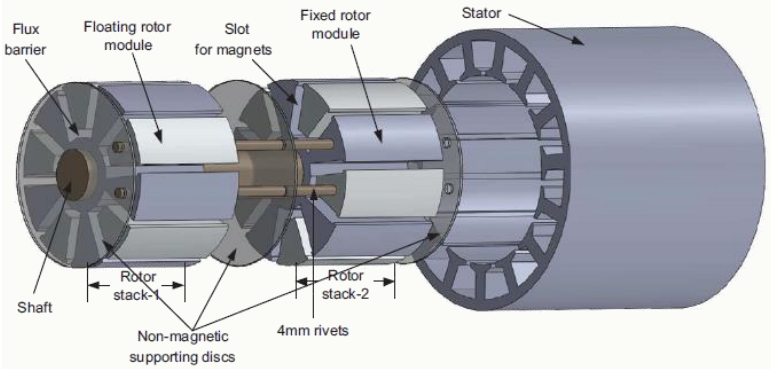

Fig. Submersible semi-modular dual stack spoke type BLDC motor

Solution:

- Ferrite magnets → low cost
- Spoke type rotor → flux concentration
- Semi Modular Dual Stack rotor
- Minimizes shaft flux leakage
- Retains rotor integrity for high speed

Fig. Hardware prototype of the BLDC motor[1].

[1] S. Sashidhar and B. G. Fernandes, "A Novel Ferrite SMDS Spoke-Type BLDC Motor for PV Bore-Well Submersible Water Pumps," in *IEEE Transactions on Industrial Electronics*, vol. 64, no. 1, pp. 104-114, Jan. 2017.

BLDC Motor and Controller for a 3 hp Solar Water (surface) Pump

- BLDC motor has 6 poles, 9 slots and is rated for 7 Nm of load torque at 3,000 RPM.
- Sensorless control is employed which reduces the component count.

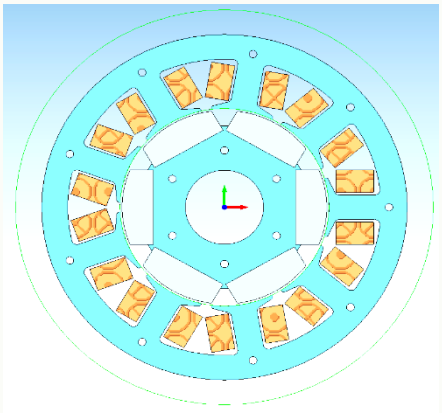

(a)

(b)

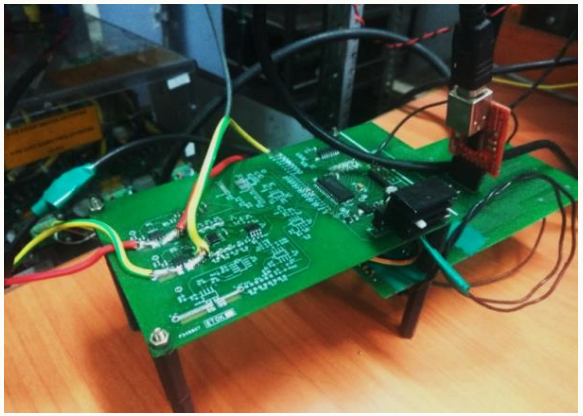

(c)

Fig. (a) FEA model of the BLDC motor, (b) Fabricated prototype of the BLDV motor is retrofitted with the Kirloskar pump, (c) The first generation PCB for drive interface and (d) the system architecture for integrating solar PV.

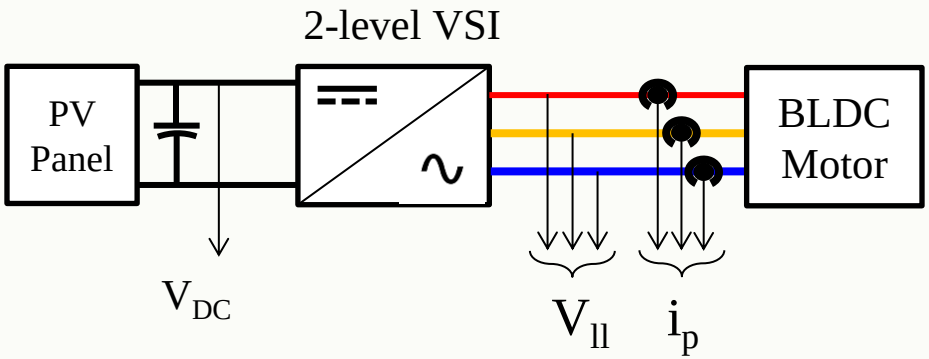

(d)

Switched Reluctance Motor for In-wheel Electric Motorcycle

- Switched reluctance motor → no permanent magnets → low cost
- Simple, robust construction, capable of operating at high temperatures

- Hub motor eliminates transmission
- Outer rotor configuration → higher torque density
- Estimated efficiency → 85%

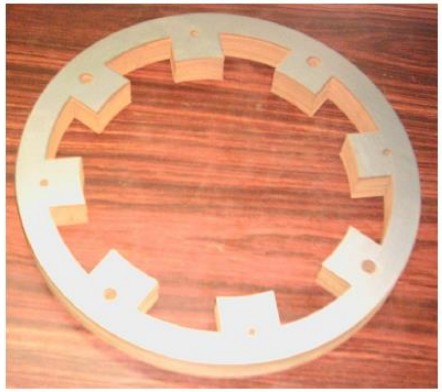

Rotor

- Prototype specifications:

Power	3 kW
Rated rpm	1000
Stator/rotor poles	6/8
Outer diameter	290 mm
axial length	130 mm

Stator laminations

Stator winding

Poly-phase Segmented Rotor SRM for Electric Vehicle

- Five phase 10/8 segmented rotor SRM[1]
  - → improves torque density
  - → improves constant power range
- Two phases conduct at a time
  - → higher torque output
  - → induces magnetic asymmetry in the motor.
- Bipolar excitation strategy
  - → eliminates magnetic asymmetry
  - → number of switches per phase remains the same (2)

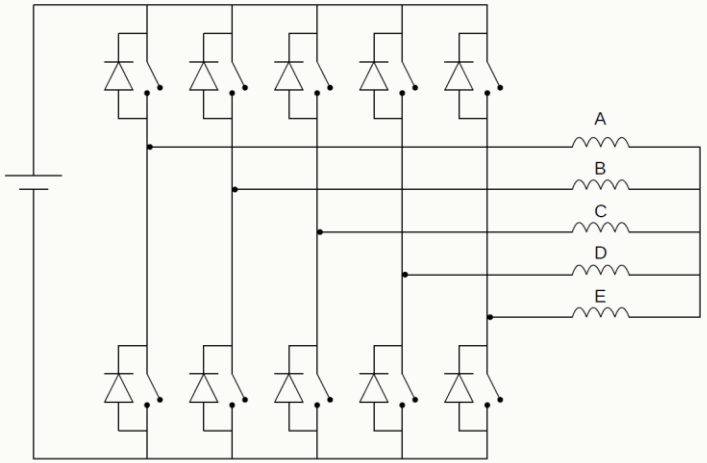

(a) 5-phase, bipolar SRM inverter

(b) Stator

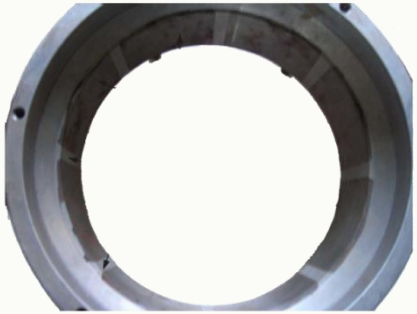

(c) Rotor

[1] R. Vandana, S. Nikam and B. G. Fernandes, "A High Torque Poly-phase Segmented Switched Reluctance Motor with Novel Excitation Strategy," IET Electric Power Applications, vol. 6, no. 7, pp. 375-384, Aug. 2012.

Concentrated Winding Segmented Rotor SRM for In-wheel EV

- Outer rotor, in-wheel SRM → Eliminates transmission and associated losses
- Low speed, high torque motor → Torque density must be improved

Salient features of the SRM:

- Segmented rotor SRM (SSRM)[1]
  → high torque density
- SSRM employees full pitch winding
  → high end winding copper loss and weight
- Thus concentrated winding SSRM is designed
  → Alternate thick and thin stator poles
- Higher number of rotor segments
  → Improves specific torque and efficiency

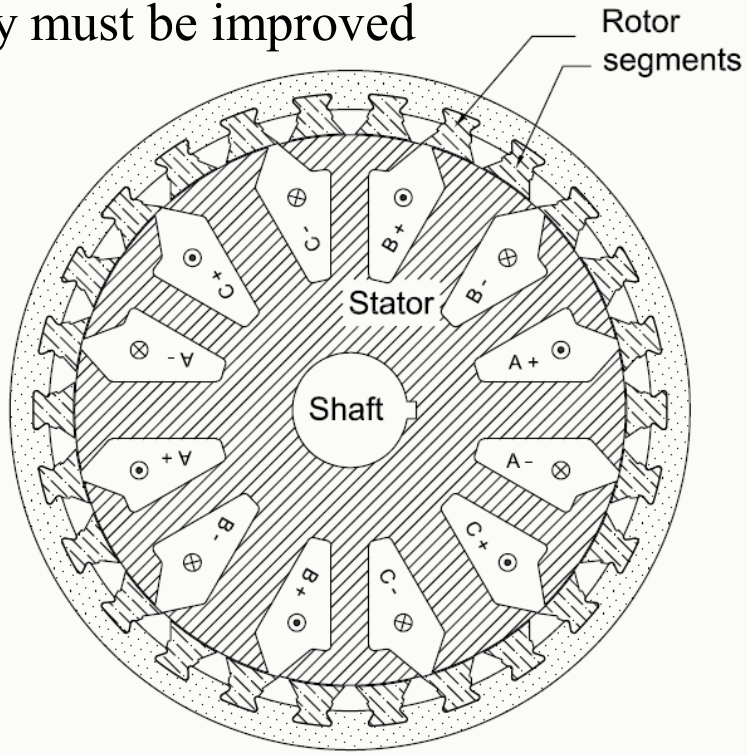

Fig. Geometry of the 12/26 segmented rotor SRM

[1] S. P. Nikam, V. Rallabandi and B. G. Fernandes, "A High-Torque-Density Permanent-Magnet Free Motor for in-Wheel Electric Vehicle Application," in *IEEE Transactions on Industry Applications*, vol. 48, no. 6, pp. 2287-2295, Nov.-Dec. 2012, doi: 10.1109/TIA.2012.2227053.

Concentrated Winding Segmented Rotor SRM for In-wheel EV

- Prototype specifications:

Torque	24 Nm @ 600 rpm
No. of Stator slots	12
No. of Rotor segments	26
Outer diameter	230 mm
Stack length	40 mm
Overall length	102 mm

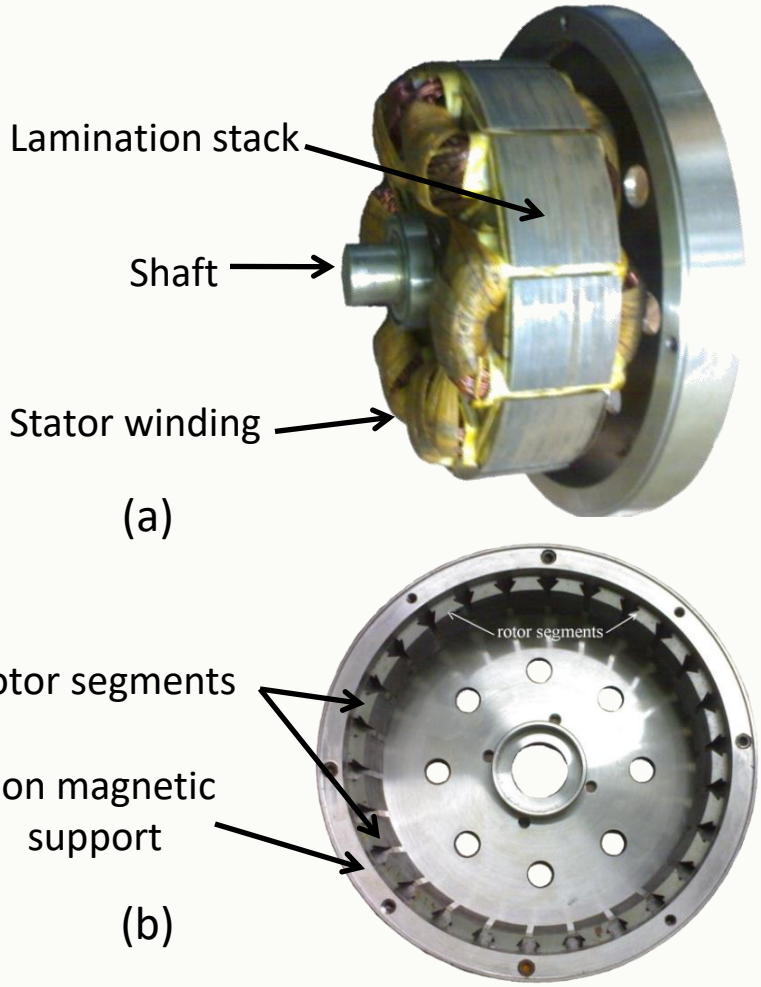

- The concentrated winding SSRM is able to achieve a maximum efficiency of 91% at 12 Nm output torque.

Fig. (a) Stator and (b) Rotor of the SSRM[2].

[2] V. R and B. G. Fernandes, "Design Methodology for High-Performance Segmented Rotor Switched Reluctance Motors," in *IEEE Transactions on Energy Conversion*, vol. 30, no. 1, pp. 11-21, March 2015.

Axial Flux Segmented Rotor Hub SRM for Electric Two Wheeler

- Axial flux motor → high torque density in large D/L ratio hub motor
- Three-phase, dual-rotor, single-stator configuration
- TORUS winding arrangement → lower copper loss
- Higher number of rotor poles than the stator slots → higher specific torque

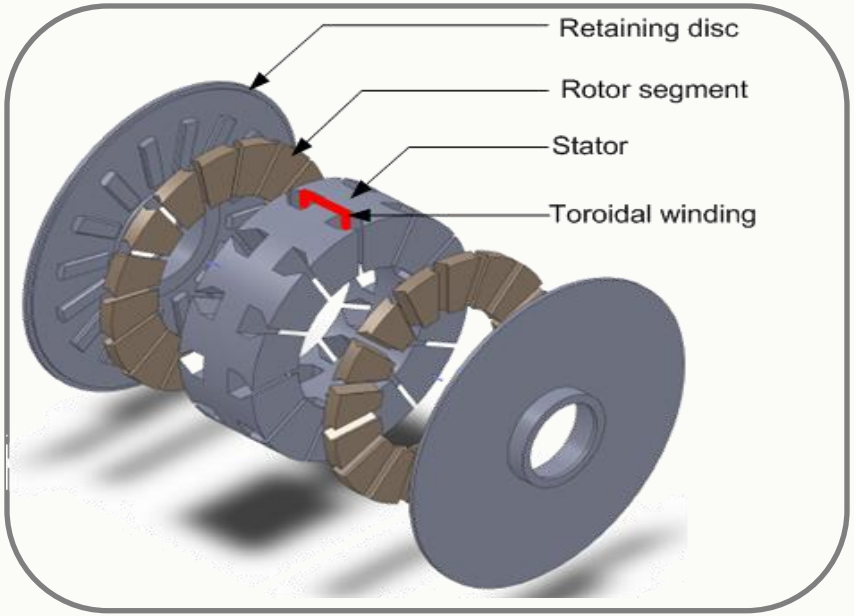

(a) Conceptual geometry

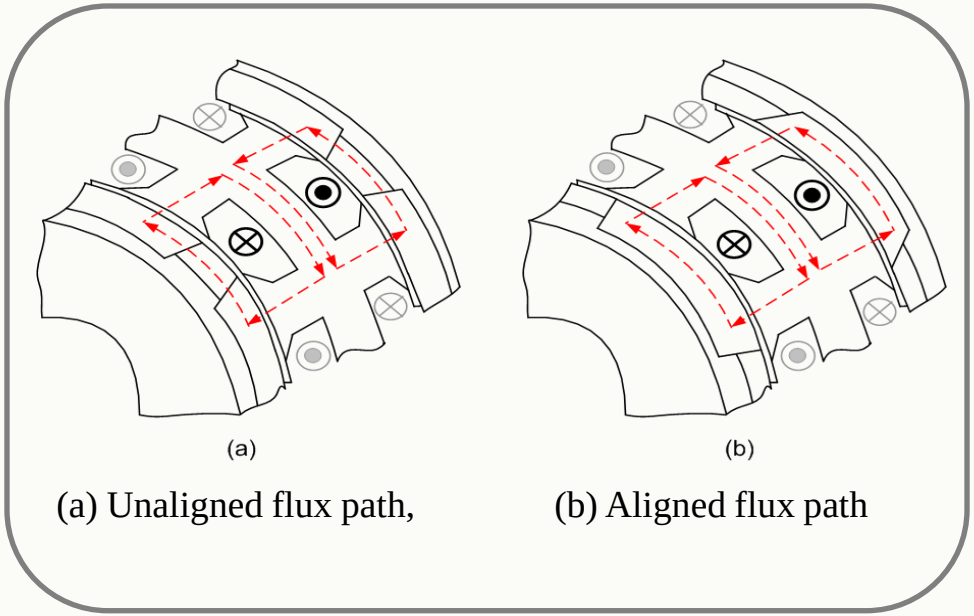

(a) Unaligned flux path, (b) Aligned flux path

(b) SRM flux paths

[1] R. Madhavan and B. G. Fernandes, "Axial Flux Segmented SRM with a Higher Number of Rotor Segments for Electric Vehicles," IEEE Trans. on Energy Conversion, vol. 28, no. 1, pp. 203-213, March 2013.

Axial Flux Segmented Rotor Hub SRM for Electric Two Wheeler

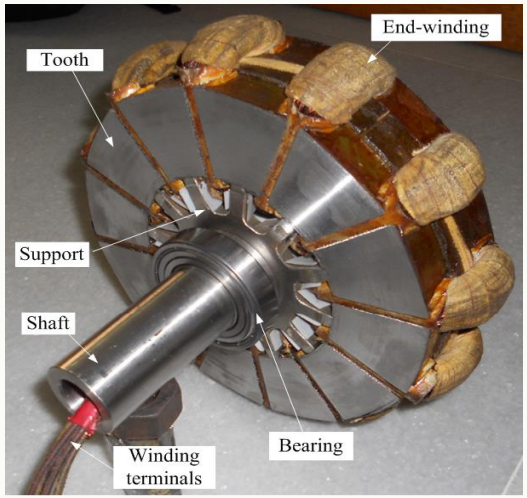

(a) Stator

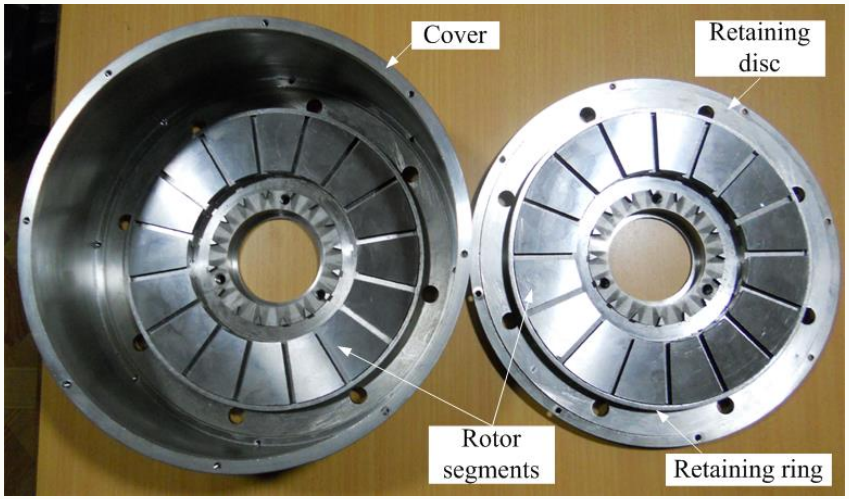

(b) Two rotors

Prototype specifications:

Rated power	1.5 kW at 600 rpm
Outer diameter	220 mm
Axial length	110 mm
Copper loss	144 W
Iron loss	43 W
Efficiency	87.5%

[2] R. Madhavan and B. G. Fernandes, "Performance Improvement in Axial Flux Segmented Rotor Switched Reluctance Motor," IEEE Trans. on Energy Conversion, vol. 29, no. 3, pp. 641-651, Sept. 2014.

Ferrite Based Permanent Magnet Motor for Electric-Assist Campus Bicycle

- 250W permanent magnet motor for Electric Assist Bicycle
- Ferrite magnets → Low cost solution
- Planetary gear → High torque capability, compact design
- High efficiency

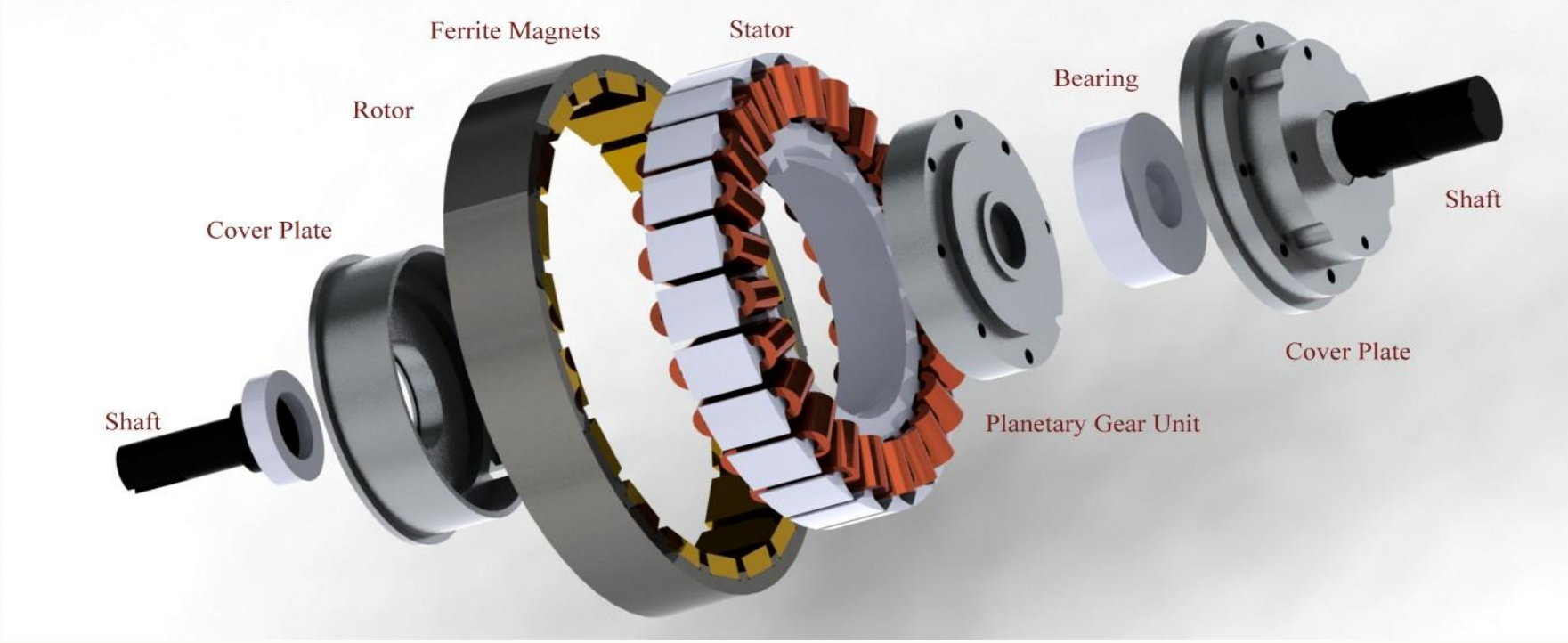

Ferrite Based Permanent Magnet Motor For Electric-Assist Campus Bicycle

- The developed prototype complete with the motor controller and battery.

High Efficiency Switched Reluctance Motor Based Ceiling Fan

- Ceiling fan is one of the most inefficient electrical appliances.
- Uses single phase induction motor
  - low cost, rugged
  - typical efficiency: 15 to 30% only
- The IM is replaced with SRM.
  - no permanent magnets / copper bars on rotor
  - robust, low cost

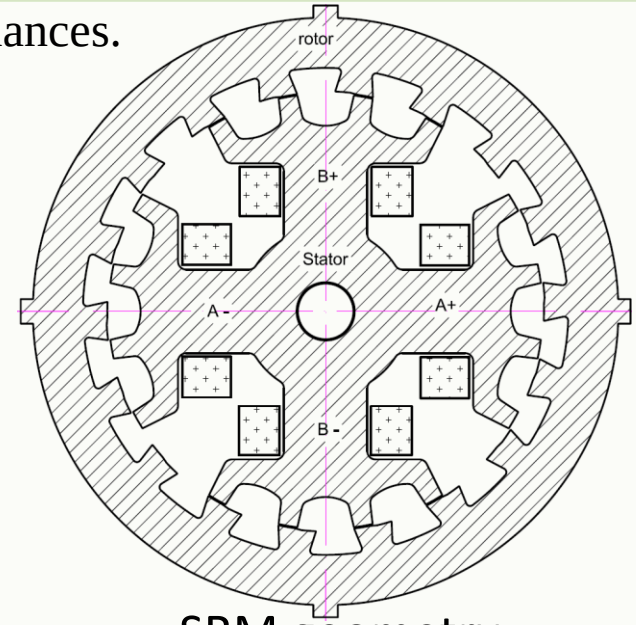

SRM geometry

Salient features of the SRM:

- Two phase design: 4 stator poles (coils)
  → low power electronic device count
- Multiple teeth (4) per stator pole
  → magnetic gearing effect: torque amplification
  → lower copper loss
- High number of rotor poles (18)
  → 16/18 pole SRM
  → higher specific torque


SRM based ceiling fan

High Efficiency Switched Reluctance Motor Based Ceiling Fan

- The SRM is driven using C-dump converter
  - → single switch and single diode per phase
  - → lower cost
- The SRM consumes 42 Watt power at rated rpm and with same blades as compared to 73 Watt of the IM.

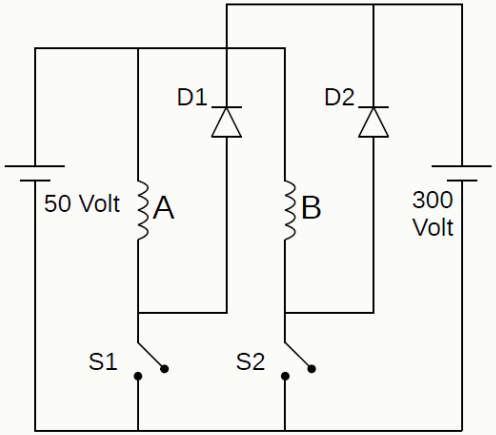

C-dump converter

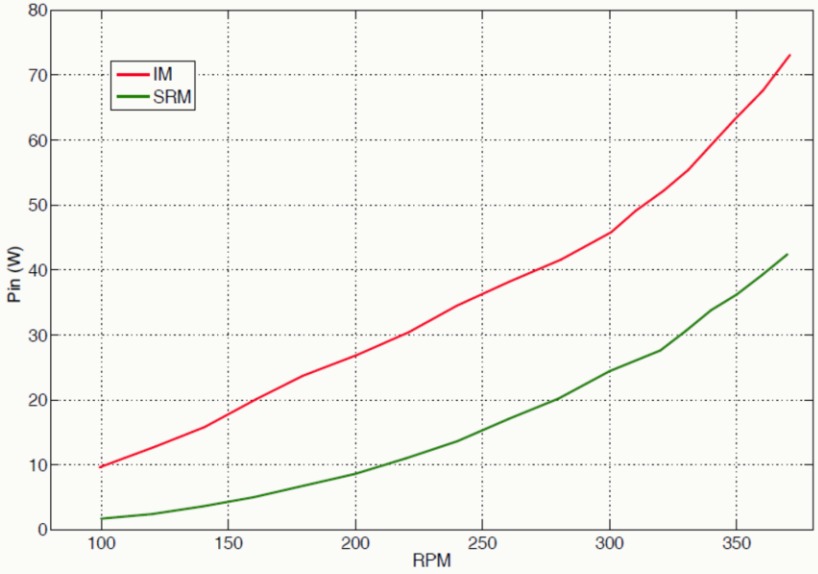

Fig. Comparison of the power intake of IM and SRM.

Rotor

Stator

Low Cost Ferrite BLDC Motor based DC Mixer Grinder for DC Micro-grids

- Operates on DC: ideal for renewable sources, DC grids
- BLDC motor: Lower power consumption
- Reduced noise, sophisticated speed control

(a)

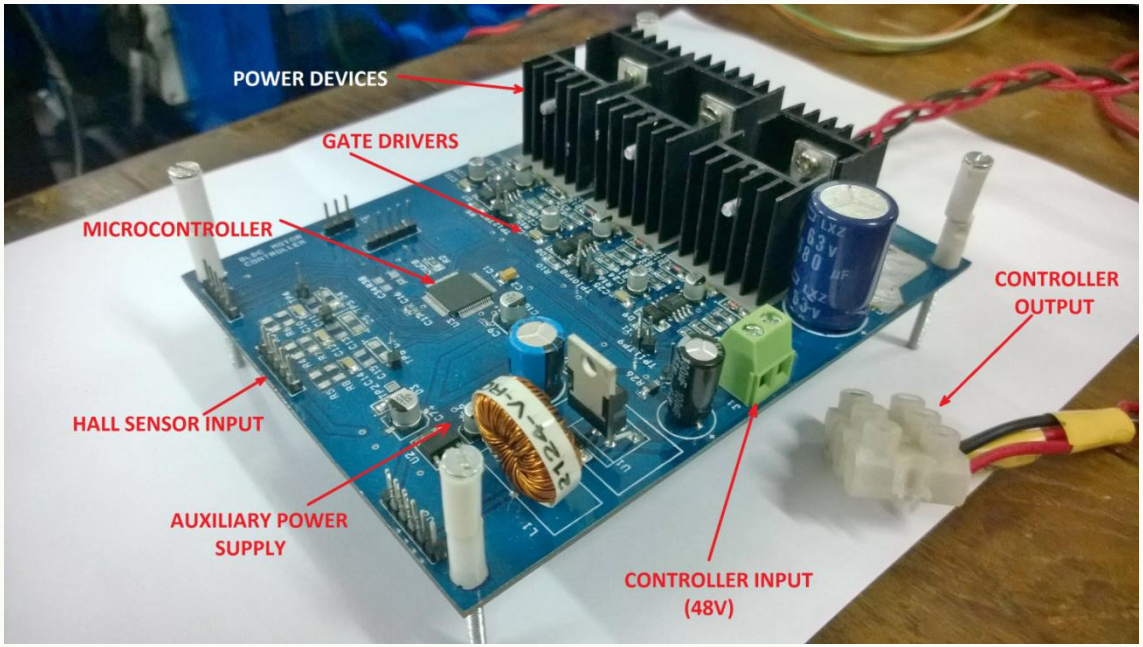

(b)

Fig. (a) The DC mixer grinder retrofitted with the BLDC motor and (b) its controller[1].

[1] C. D. Bhagat, S. P. Nikam and B. G. Fernandes, "Design and development of sensorless controller for DC-operated mixer-grinder," SGBC *2016*, 2016, pp. 1-6, doi: 10.1109/SGBC.2016.7936065.

Permanent Magnet DC Motor Directly Powered by PV Panel

- Coarse MPPT operation is performed without using a power electronic converter.

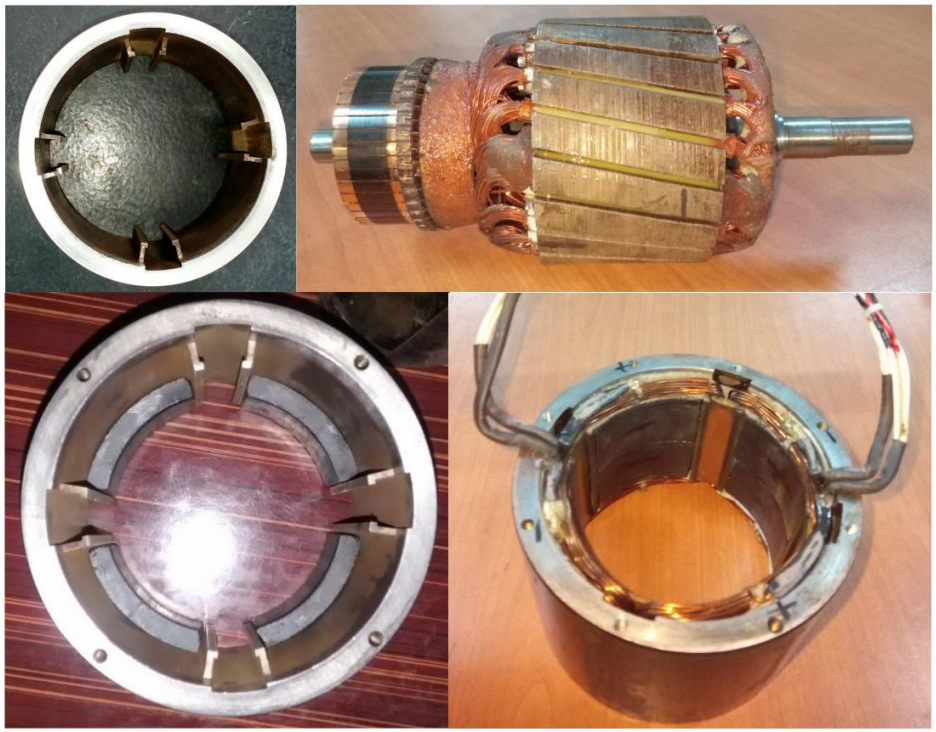

(a)

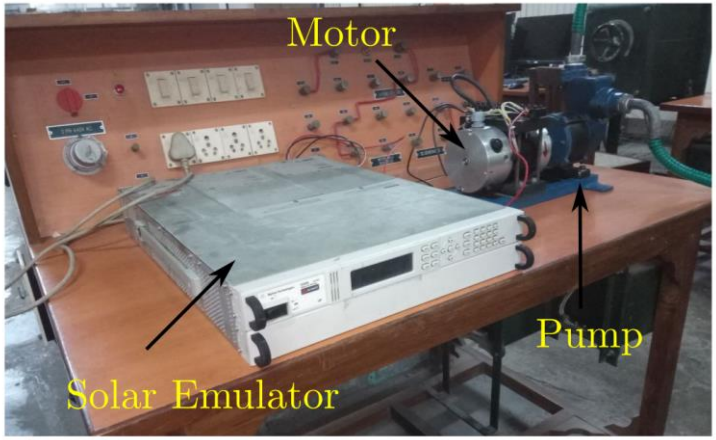

(b)

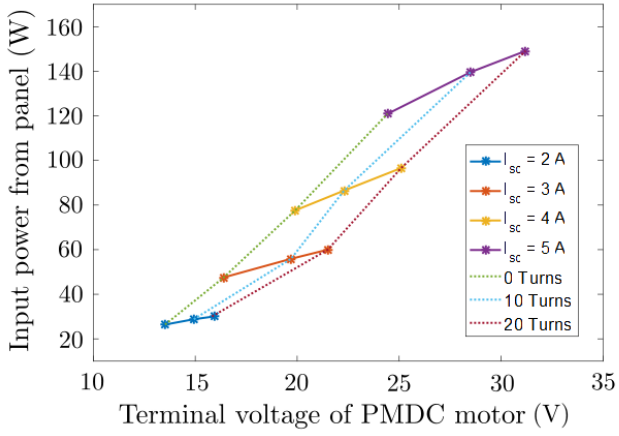

(c)

Fig. (a) Stator, rotor and yoke of the experimental prototype before the final assembly, (b) The experimental setup and (c) the measured voltage vs. power (V-P) characteristics.

Magnetic Gear Integrated Segmented Rotor Switched Reluctance Motor

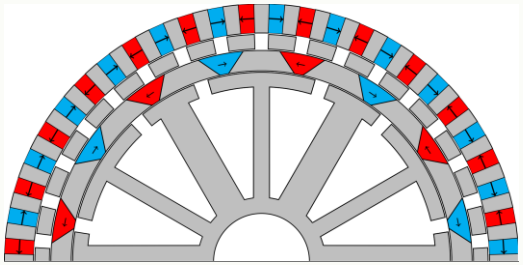

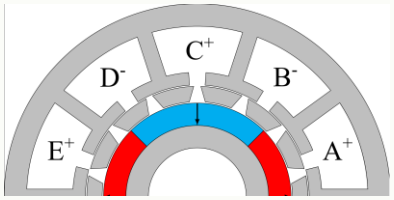

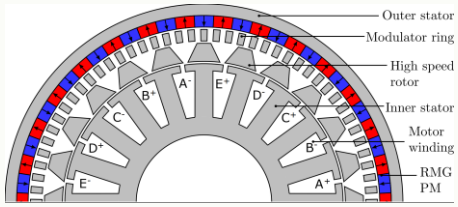

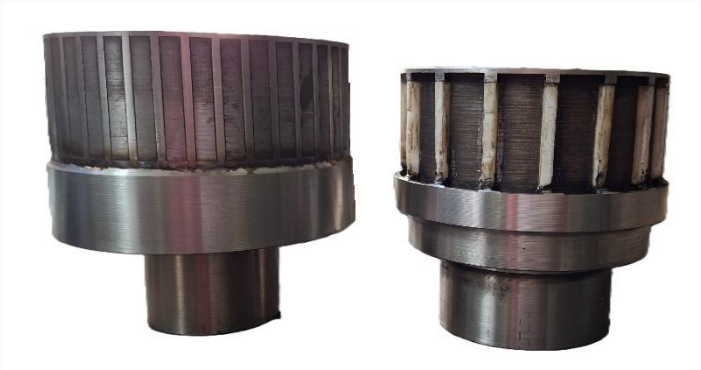

- High torque density hub motor for EV → 3.3 kW, 40 Nm.
- Contact energy transfer through magnetic gearing action
- India's first magnetic geared motor
- World's first magnetic geared SRM
- A completely PM free geared SRM topology has been developed.
- A geared SRM with only 3 members has been developed.

More details: https://sites.google.com/view/saptarshidey

Condition monitoring of electrical machines using vibration signatures

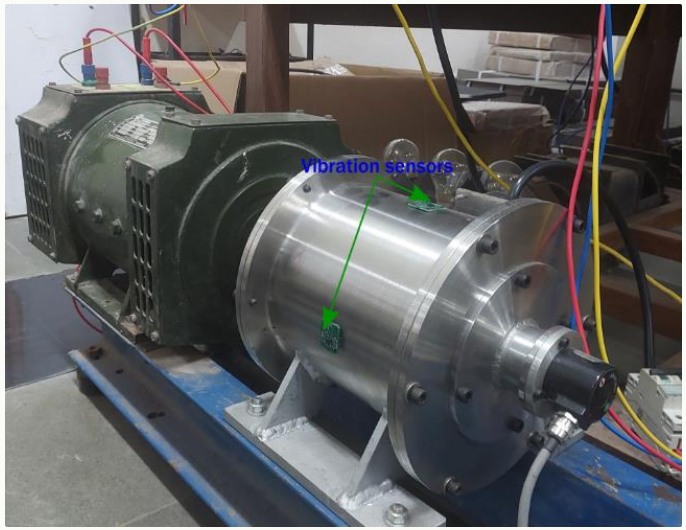

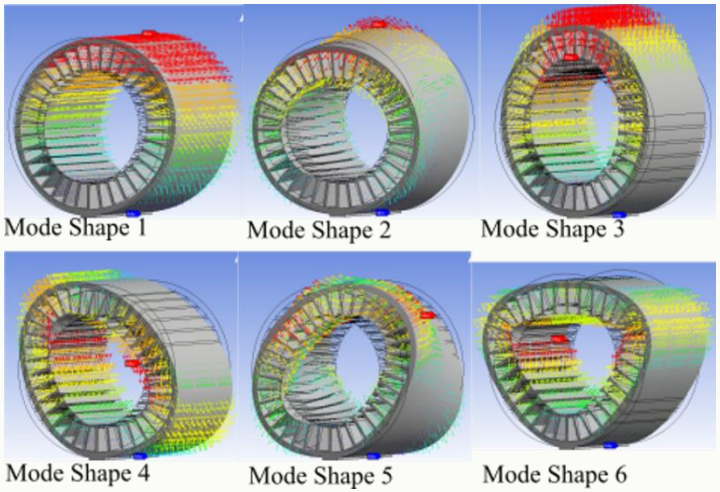

- Experimental test rig with 1.5 kW, 750 RPM IPM and SPM type PMSMs developed in-house.
- Accurate fault detection using vibration signatures.
- Strategic placement of vibration sensors for maximum utilization of the sensors.
- Correlating vibration with air-gap flux density distribution.
- Capable of detecting faults in the rotor as well as the armature.

1. S. Sengupta, N. Endla, A. Kushwaha and B. G. Fernandes, "Modelling and Analysis of PM Demagnetization and its Effect on Vibration in SPM Machines," *2023 IEEE 14th International Symposium on Diagnostics for Electrical Machines, Power Electronics and Drives (SDEMPED)*, Chania, Greece, 2023, pp. 377-382.
2. S. Sengupta and B. G. Fernandes, "Impact of Electric and Magnetic Loading on the Electromagnetic Stress of PM Machines," *2024 International Conference on Electrical Machines (ICEM)*, Torino, Italy, 2024, pp. 1-7, doi: 10.1109/ICEM60801.2024.10700136.

Segmented-Rotor Hybrid-Excited Synchronous Motor for EV Applications

(a)

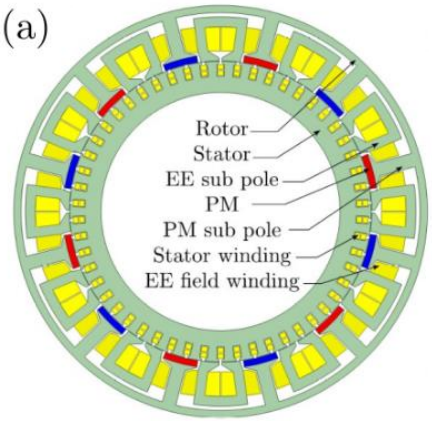

Particulars	Units	Values
Rated, peak output power	W	3392, 6535
Rated, peak torque	N·m	41, 79
Rated, maximum speed	rpm	790, 2370
Maximum efficiency	%	96
Peak torque density	$N·m/dm^3$	25
	N·m/kg	5.5
Rated torque density	$N·m/dm^3$	13
	N·m/kg	2.9
Peak power density	W/dm^3	2068
	W/kg	457
Rated power density	W/dm^3	1073
	W/kg	237.2
Peak torque/PM mass	N·m/kg	181
Rated torque/PM mass	N·m/kg	94

(b)

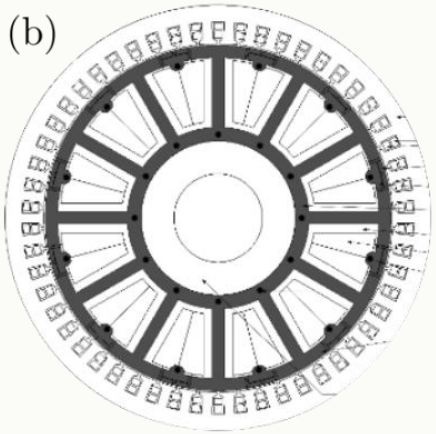

Particulars	Units	Values
Peak power	kW	254
Continuous power	kW	105.5
Peak torque	Nm	405
Continuous torque	Nm	168
Peak power density	kW/dm^3	67.7
	kW/kg	11
Continuous power density	kW/dm^3	28
	kW/kg	4.6
Peak torque density	Nm/dm^3	108
	Nm/kg	17.6
Continuous torque density	Nm/dm^3	44.8
	Nm/kg	7.3
Peak torque/PM mass	Nm/kg	508.8
Continuous torque/PM mass	Nm/kg	211
Maximum efficiency	%	96.4

- Electrically excited rotor → capable of large field weakening as well as increasing torque capability.
- Electrically excited rotor → no slip ring-brush gear arrangement → robust and fault tolerant
- Rotating transformer

1. S. Dey and B. G. Fernandes, "A Novel Segmented-Rotor Hybrid-Excited Synchronous Motor for Electric Vehicle Application," *2024 International Conference on Electrical Machines (ICEM)*, Torino, Italy, 2024, pp. 1-7, doi: 10.1109/ICEM60801.2024.10700216.

Very High-Speed (100 krpm) Induction Motor for Spindle Applications

- Novel rotor bar shape → enhances torque density by 13% and satisfies the mechanical stress constraints.
- Hybrid rotor: copper rotor bar and aluminium 7075 alloy end-ring
- Stator slots - 18, rotor bars - 24, slip - 0.6\%.
- Specs: 40 mNm, 450 W, 2-pole, 100 kRPM
- Novel rotor → high conducting material for rotor bars and high strength alloy for end rings for reducing mechanical stress.

1. S. Mathew, R. M. R. Kumar, N. K. Endla, C. Vundru, R. Singh and B. G. Fernandes, "Development of a Hybrid Rotor Structure for high-speed Laminated Rotor Induction Motor," *2021 IEEE International Electric Machines & Drives Conference (IEMDC)*, Hartford, CT, USA, 2021, pp. 1-7, doi: 10.1109/IEMDC47953.2021.9449519.
2. S. Mathew, R. M. Ram Kumar and B. G. Fernandes, "A novel rotor bar shape for enhancing the torque density of high-speed induction motor," *2020 International Conference on Electrical Machines (ICEM)*, Gothenburg, Sweden, 2020, pp. 2365-2371, doi: 10.1109/ICEM49940.2020.9270647.

3.5 kW, 60,000 RPM High Speed Syn. Rel. Machine for Electric Assist Turbocharger

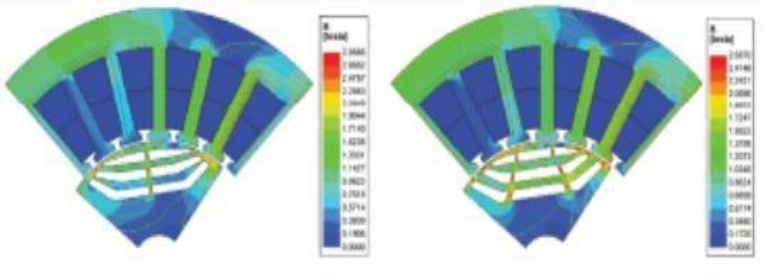

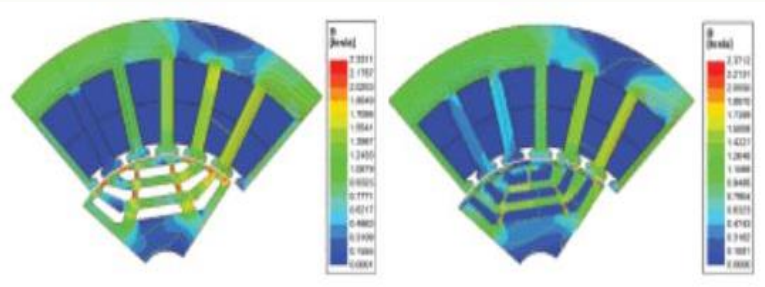

- High speed synchronous reluctanc e rotor is designed using high strength Martensitic sleeve.
- Optimized sleeve rotor → produces 4.5% and 46.7% higher torque in comparison to SynRel machines using high and low strength laminations with conventional rotor configurations.
- Nearly 90% by volume of the conventional rotor lamination

1-ϕ Line Start Synchronous Reluctance Motor

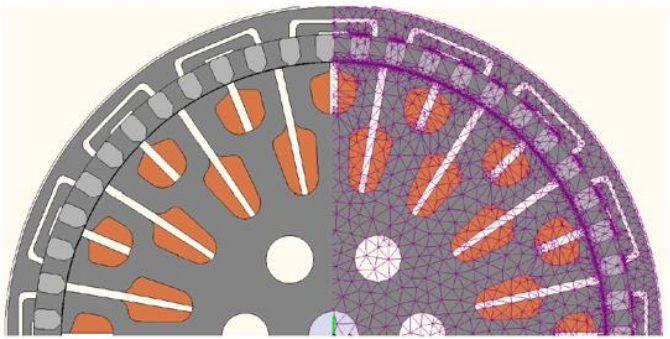

- Pin < 38 W, Ns < 375 RPM, Air delivery > 220 CMM.
- Outer rotor with a high number of poles
- Asymmetric rotor cage-barrier combination
- Reduced ohmic loss in the rotor
- Highest efficiency among the PM and PE converter-free ceiling fan motors.

PM-assisted SyRM for Submersible Pumps

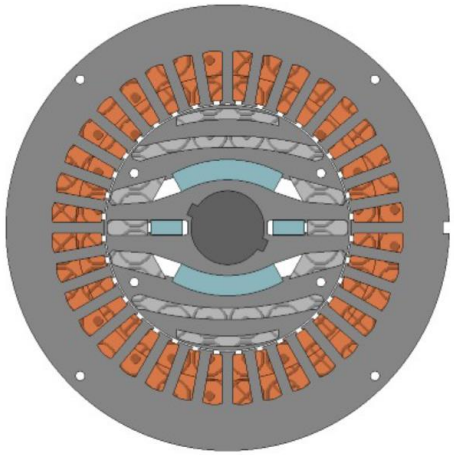

Line-Start at lower voltage and less prone to demagnetization

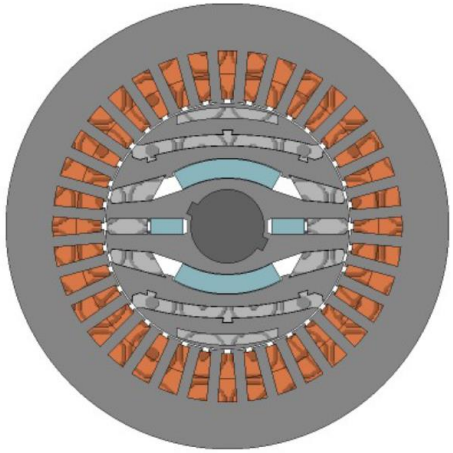

New Rib-less Configuration With Enhanced Torque Density

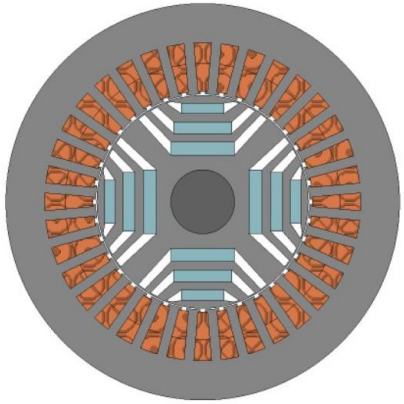

Rectangular magnets

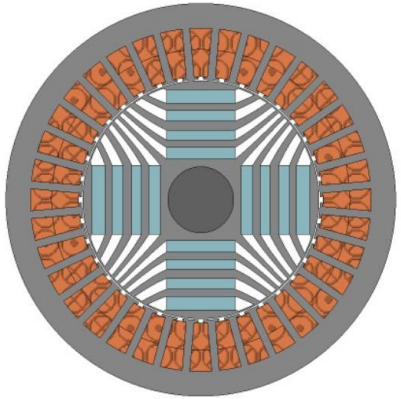

Semi-fluid Barrier with Rectangular Inner Magnets

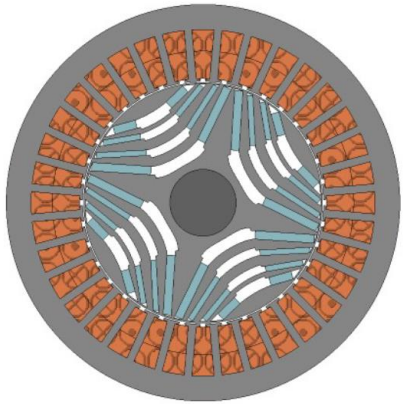

Semi-fluid Barrier with Rectangular Side Magnets

Synchronous Reluctance Motors for EV Applications

Design parameters	Value
DC link voltage	48 V
Core length	80 mm
Stator OD	140 mm
Base speed	3000 rpm
Peak speed	9000 rpm
Active volume	1.3 L
Active weight	8.4 kg
CPSR	1:3
Peak/Rated Power	6 kW/3kW
Peak/Rated Torque	20 Nm/10 Nm

Ferrite IPM-SyRM prototype for electric 2W

Design parameters	Value
Axial length	180 mm
Outer diameter	157 mm
Power	2 kW
Volume	3.5 L
Weight	11 kg

Ferrite IPM-SyRM prototype for electric 3W

Motor Integrated Rotating PM Based Electrodynamic Suspension Device (MIEDW)

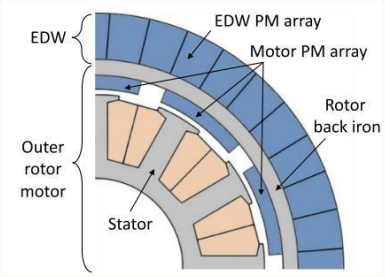

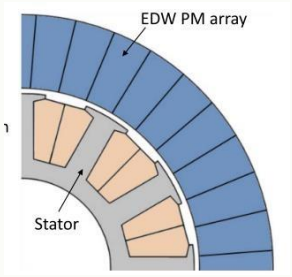

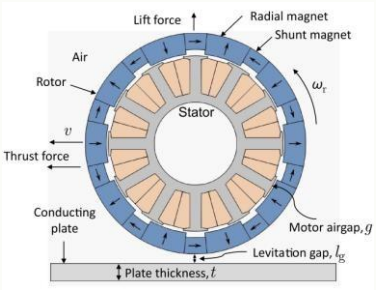

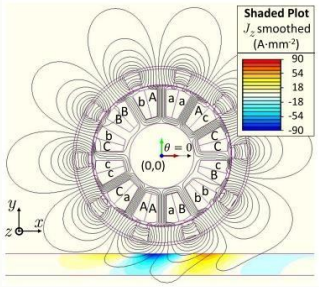

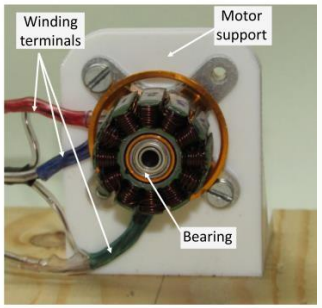

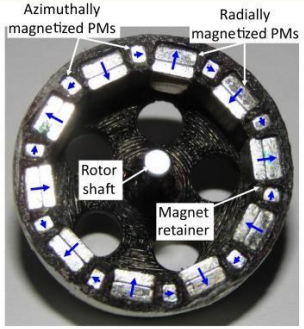

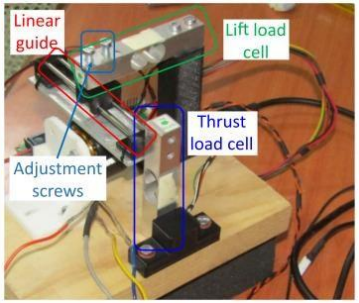

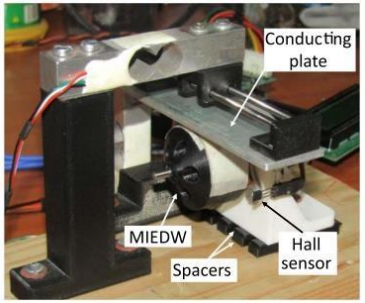

- The proposed MIEDW offers key advantages → improved utilization of PM and active material, and higher full-load and maximum efficiencies
- The MIEDW with cage rotor structure to retain the magnets is electromagnetically and structurally superior → this offers 8.8% higher lift-to-magnet weight ratio as compared to the rotor with only shell supports, for the same physical clearance.

A. Kushwaha, N. Endla and B. G. Fernandes, "Motor Integrated Rotating Permanent Magnet Based Electrodynamic Suspension Device: Part I— Concept and Comparison," in *IEEE Transactions on Energy Conversion*, vol. 38, no. 3, pp. 1701-1714, Sept. 2023, doi: 10.1109/TEC.2023.3270342.

Dual-motor Two-wheeled Electric Vehicle Chassis-mounted Traction Motor (3kW PMSM)

- A dual motor topology offers the following benefits
  - Efficient operation in various operating regions, e.g. acceleration, coasting, etc.
  - Improvement in regeneration efficiency.
- Relevant specifications of the inner rotor motor
  - Base speed: **1800** RPM
  - Max. speed: **5000** RPM
  - Max. torque: **16** Nm
  - No. of slots: 12
  - No. of poles: 10

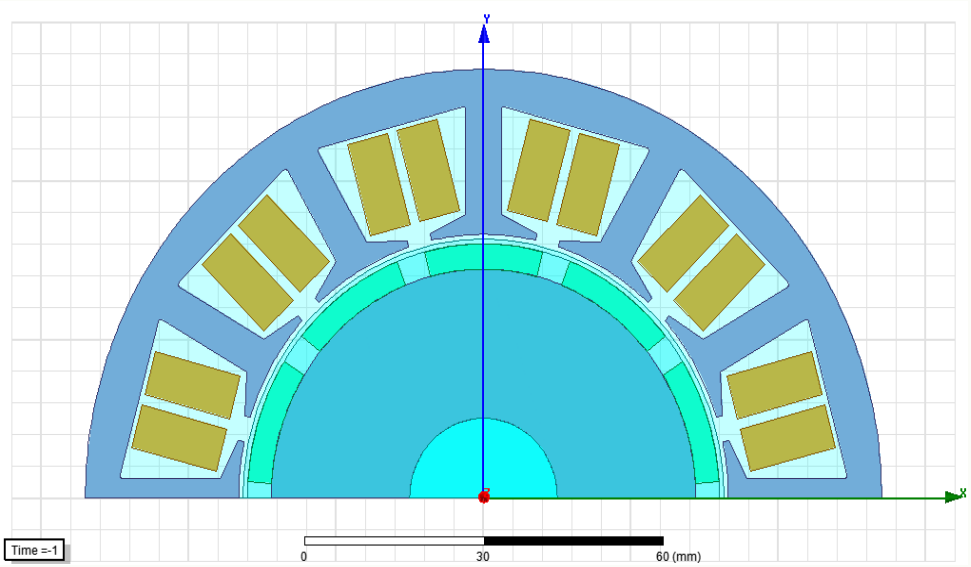

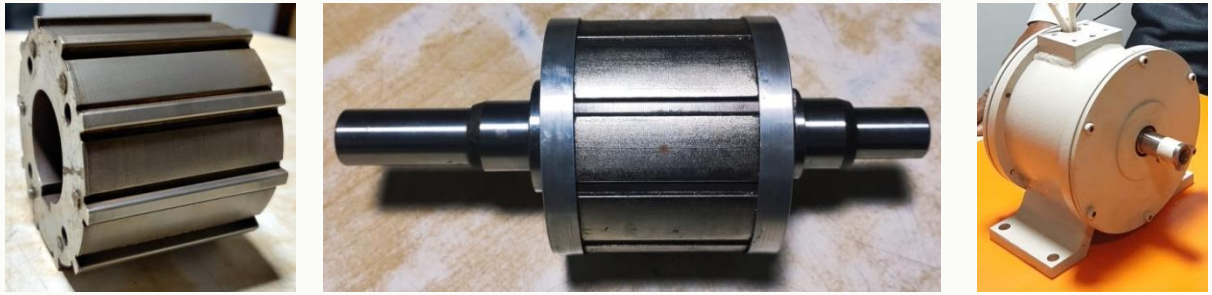

Fig. FEM model, stator, rotor and the final assembly of the manufactured prototype.

Dual-motor Two-wheeled Electric Vehicle Hub-mounted Traction Motor (1.5 kW PMSM)

- A dual motor topology offers the following benefits
  - Efficient operation in various operating regions, e.g. acceleration, coasting, etc.
  - Improvement in regeneration efficiency.
- Relevant specifications of the inner rotor motor
  - Base speed: **600** RPM
  - Max. speed: **1000** RPM
  - Max. torque: **24** Nm
  - No. of slots: 12
  - No. of poles: 10

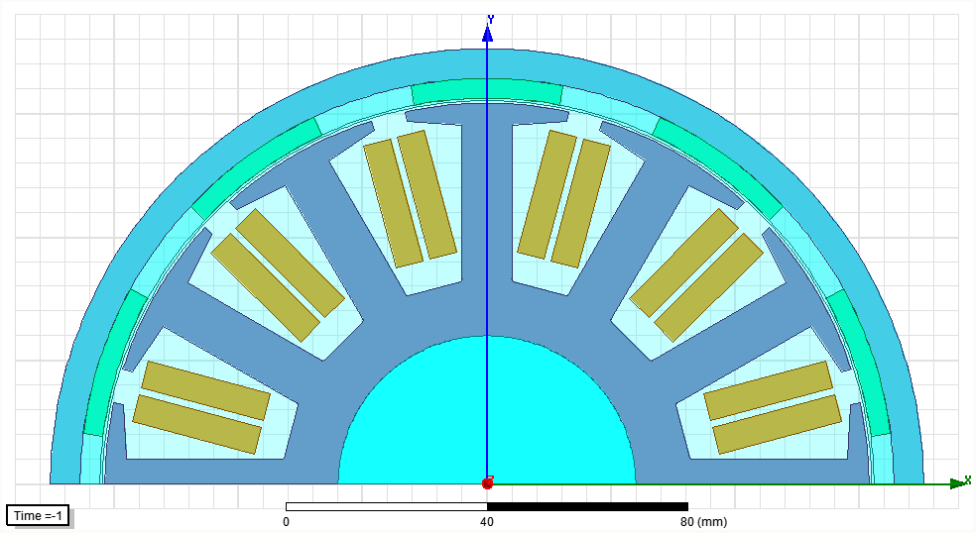

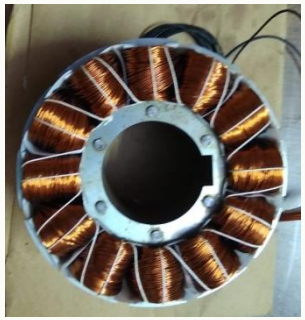

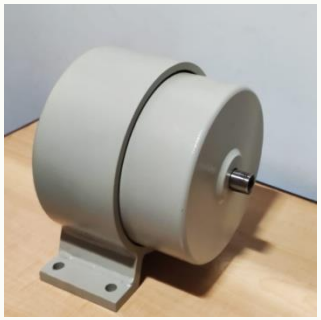

An OVERVIEW of Research and Development Activities in GaN based PE Converter, Integration of RES in Microgrid, High-power Converter, and SST

PEPS, EE Department,

IIT Bombay

GaN Based Interleaved Isolated Boost Converter

- Interleaved boost converter to boost 48 V to 400 V.
- Planar magnetics is used to reduce height and obtain low profile.

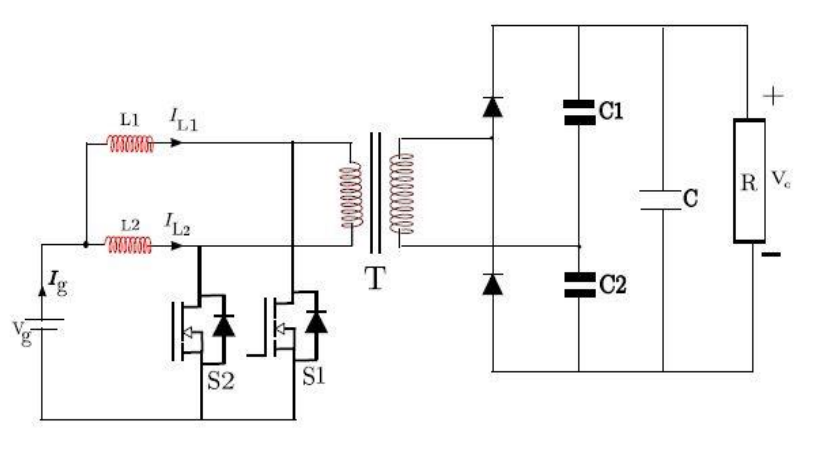

(a)

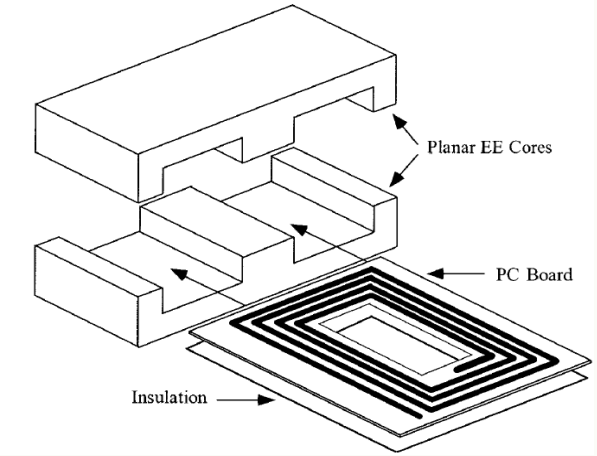

(b)

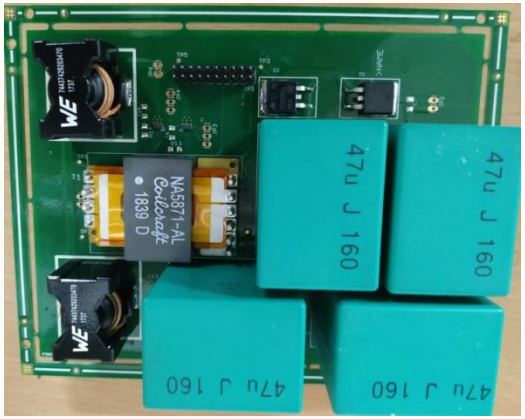

(c)

Fig. (a) Schematic of proposed interleaved isolated boost converter[1], (b) Planar transformer core and PCB winding, and (c) the fabricated converter assembly.

[1] S. Akshatha, R. Vinayak and B. G. Fernandes, "Isolated Dual Boost Converter: Controller Design using Affine Parameterisation," PEDES 2018, pp. 1-6, doi: 10.1109/PEDES.2018.8707597.

GaN Based Half-bridge DC-DC converter for Ultracapacitor Interface

- Switching frequency is 1MHz.
- Power Circuit, controller and sensing are incorporated on a single PCB.

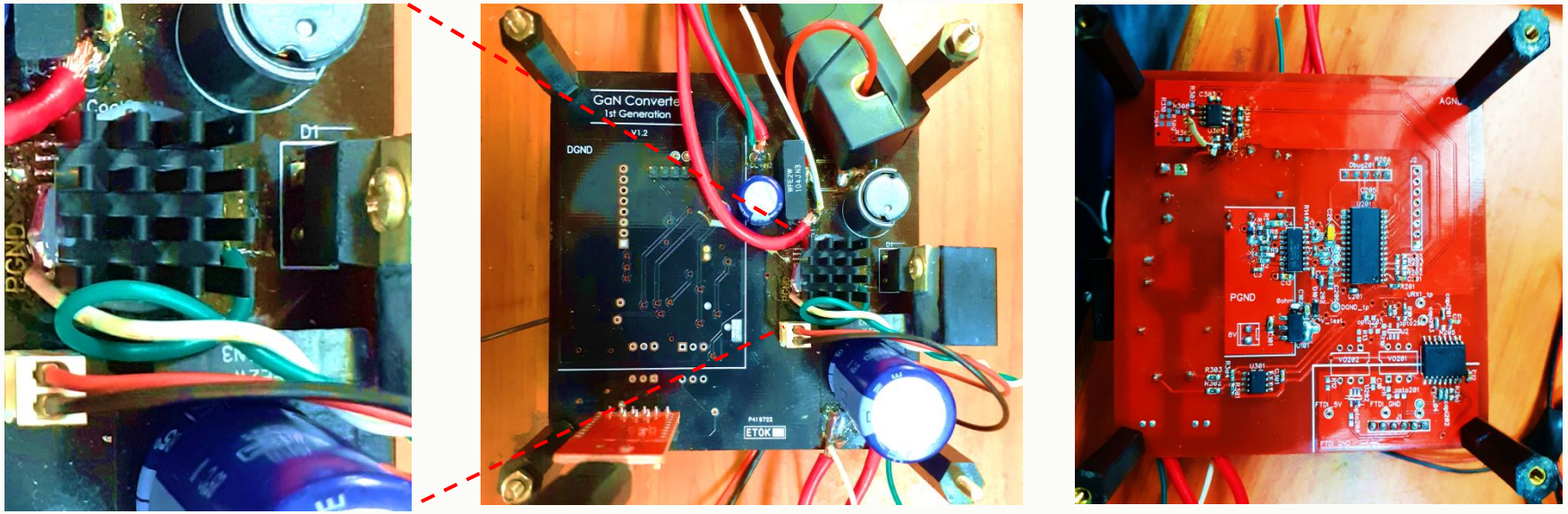

(a) (b) (c)

Fig. (a) Zoomed view of the GaN device (Infineon CoolGaN series GaN HEMT) along with its heatsink, (b) Top and (c) Bottom views of the fabricated PCB.

GaN Based Half Bridge Leg Designed for 1 kW Totem pole PFC

- 4 layer PCB is adapted; TI's integrated GaN IC has been used to further reduce the parasitic inductance.
- Power Circuit, controller and sensing are incorporated on a single PCB.
- Converter ratings: Input voltage (rms) (115 v – 230 V), Ouput voltage (390 V), Output power (1 kW), Switching frequency (100 kHz),

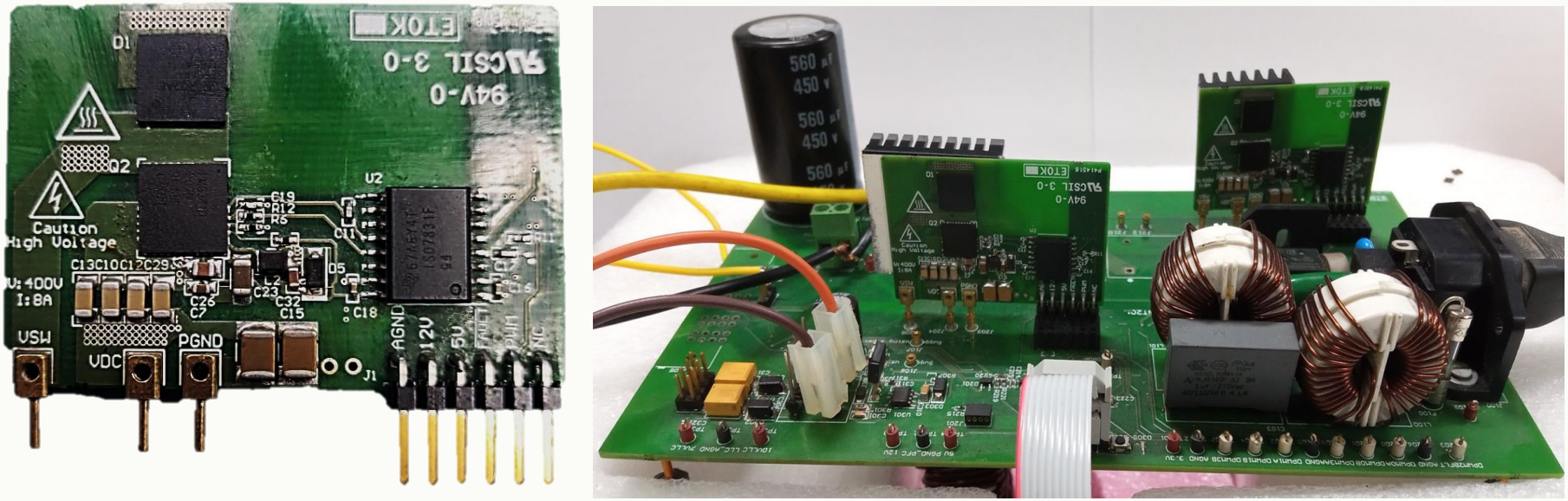

(a) (b)

Fig. (a) GaN device (TI GaN HEMT: 600 V, 12 A, Rdson = 12 mΩ) based half bridge leg and (b) the fabricated converter assembly for 1 kW bridgeless PFC.

An OVERVIEW of Research and Development Activities in GaN based PE Converter, Integration of RES in Microgrid, High-power Converter, and SST

PEPS, EE Department,

IIT Bombay

Unified controller for OV Prevention, Islanding Detection and LVRT at High Penetration of PV in Low Voltage Grid

- Unified controller for voltage regulation and islanding detection for feeders with low reactance to resistance (X/R) ratio.

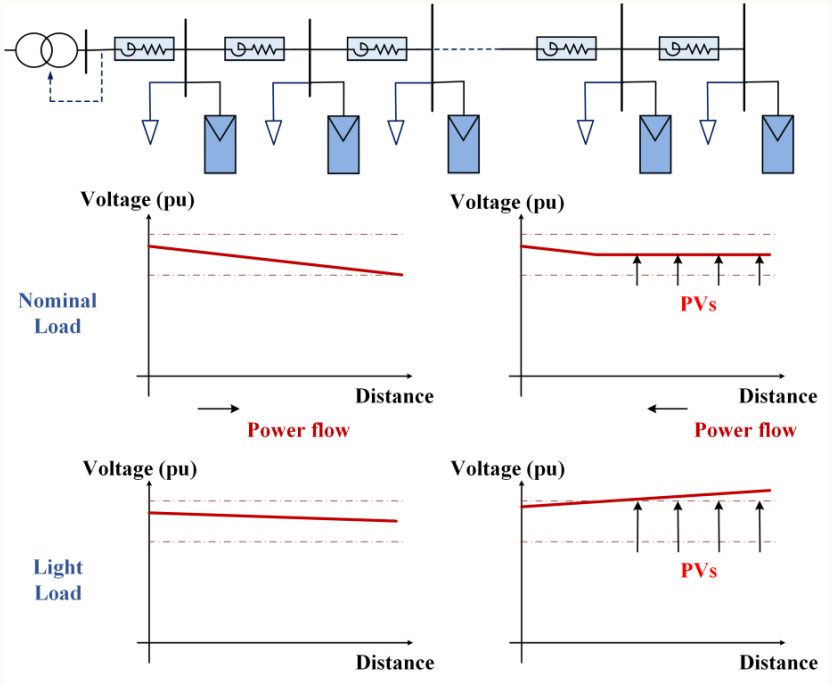

(a)

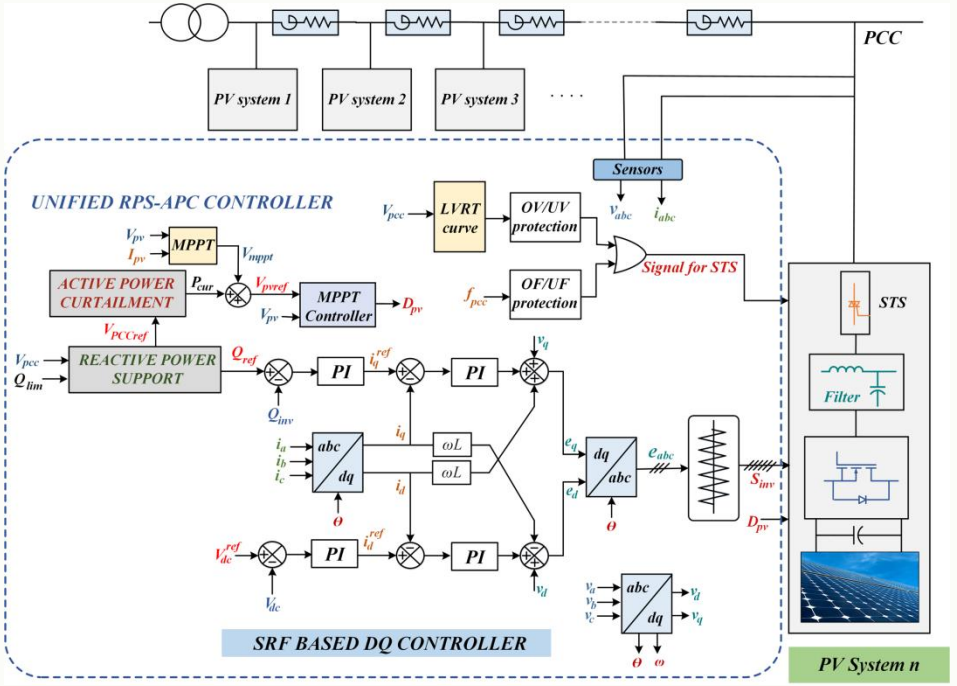

(b)

Fig. (a) High penetration of PV in a low voltage grid, and (b) Unified RPS-APC controller[1].

[1] H. Khan, B. G. Fernandes and A. Kulkarni, "Unified controller for overvoltage prevention, Islanding detection and LVRT at high penetration of PV systems connected to a LV grid," IAS *2017*, Chicago, IL, 2017, pp. 1-5.

Decoupled Controller for Simultaneous Harmonic and Unbalance Compensation in a RES system in a Low Voltage Grid

- Low-voltage ride through (LVRT) controller, DDSRF-based PLL for grid synchronization and sequence extraction from unbalanced grid voltages.
- Proportional- resonant (PR) based controller for injection of unbalanced currents.

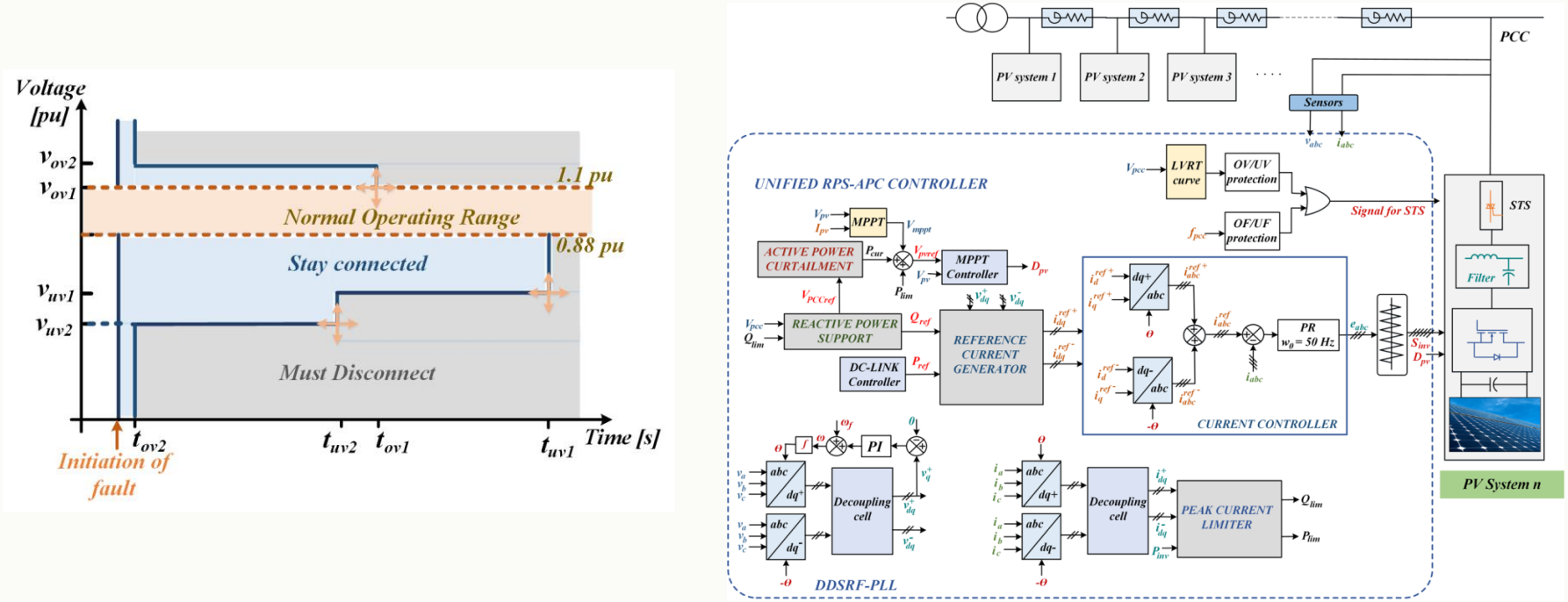

Fig. (a) Standards for islanding detection, and (b) Unified RPS-APC controller[1].

[1] H. Khan, S. J. Chacko, B. G. Fernandes and A. Kulkarni, "An integrated controller to perform LVRT operation in PV systems connected to a LV grid during balanced and unbalanced faults," ECCE Asia *2017*, Taiwan, pp. 2002-2007.

An Integrated Controller to Perform LVRT Operation in PV Systems in a Low Voltage Grid During Balanced and Unbalanced Faults

- Hybrid controller for unbalance, neutral and harmonic compensation.
- Interfacing converters in RESs can suffice neutral current compensation and harmonic compensation simultaneously.
- Multifunctional renewable energy storage (RES) systems.

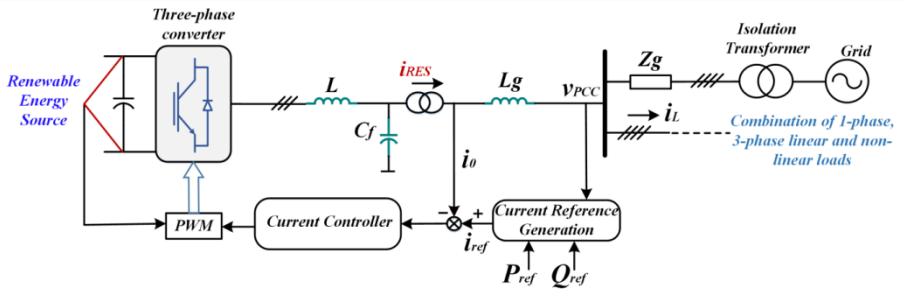

(a)

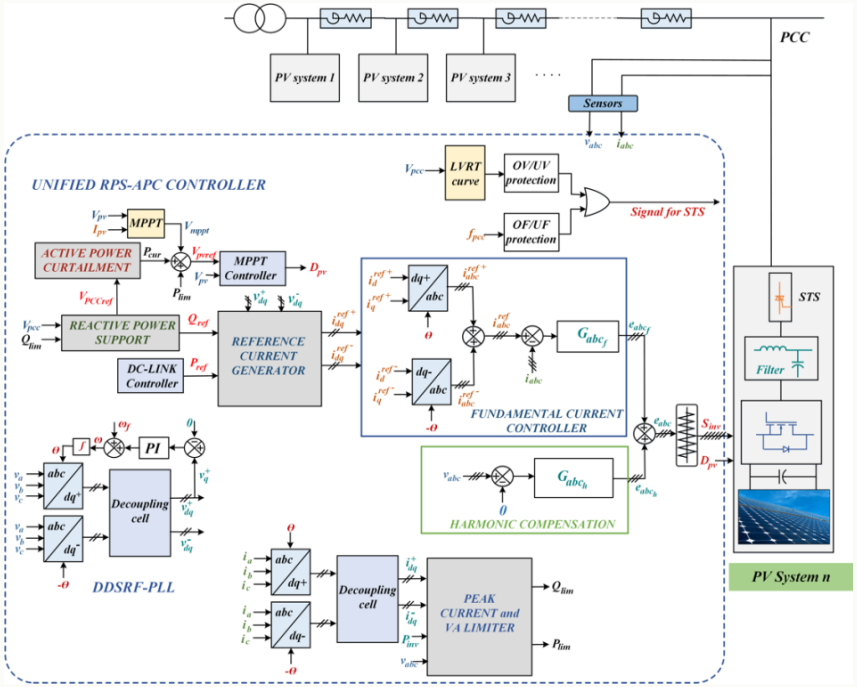

(b)

Fig. (a) Renewable energy source (RES) connected in a low voltage distribution grid, and (b) Unified RPS-APC controller[1].

[1] H. Khan, B. G. Fernandes and A. Kulkarni, "Decoupled Controller for Simultaneous Harmonic and Unbalance Compensation in a multifunctional RES system connected to a LV Distribution Grid," EPE *2018,* Riga, Latvia.

Integration of Low-voltage PV With AC Grid Employing a Unified AC-DC System

- Integration of a renewable energy source (RES) with ac grid is examined using a three-phase PWM rectifier and low voltage (LV) photovoltaic (PV).[1,2]
- It introduces multifunctionality using a single PWM converter.

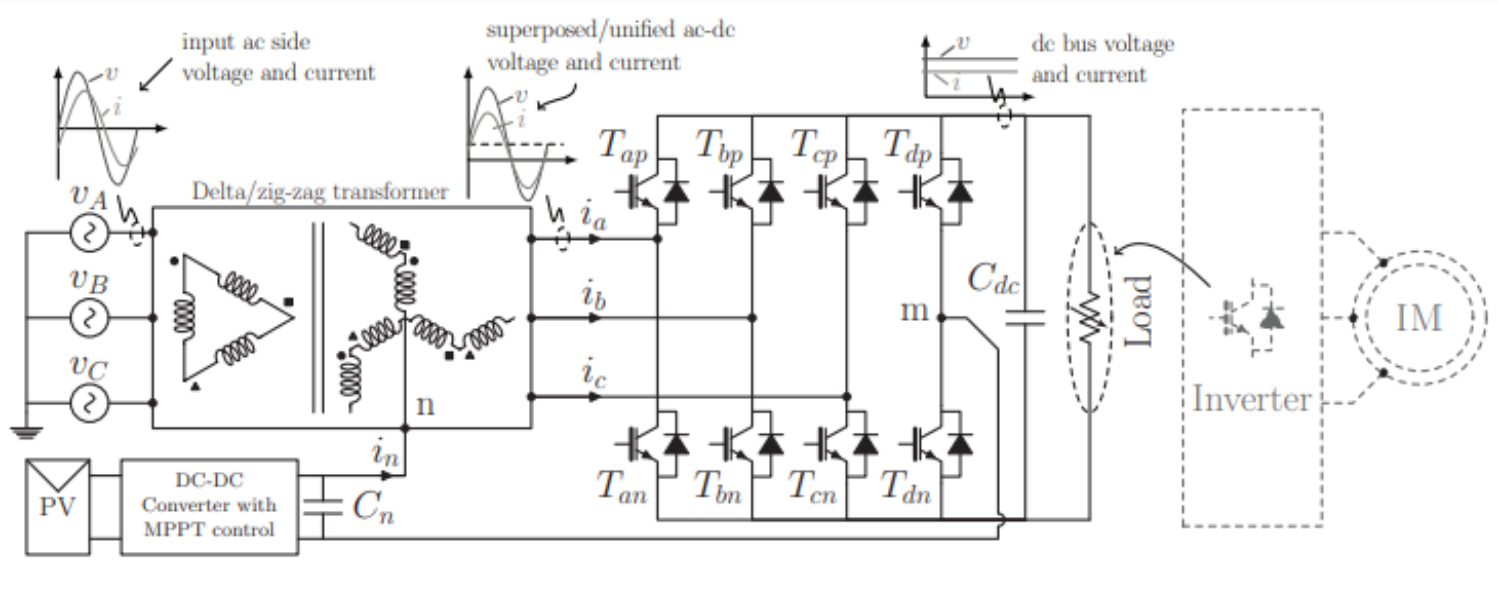

Fig. The proposed scheme uses a line-frequency zig-zag transformer and a single three-phase four-leg PWM rectifier to integrate the low voltage PV with three-phase ac grid.

[1] A. Shetty, B. G. Fernandes, O. Ojo, and J. A. Ferreira, "Low-voltage pv power integration for variable frequency drives application," in EPE 2017, Sept 2017, pp. P.1–P.10.

[2] V. Chitransh, A. Shetty, A. K. Das, J. O. Ojo, M. Veerachary, B. G. Feranandes and J. A. Ferreira, "Evaluation of Multifrequency Power Electronic Converters: Concept, Architectures, and Realization," in *IEEE Journal of Emerging and Selected Topics in Power Electronics*, vol. 9, no. 3, pp. 3582-3597, June 2021, doi: 10.1109/JESTPE.2020.3019730.

Design Methodology of a Line-frequency Zig-Zag Transformer in a Unified AC-DC System

- Overall power density of the UACDC converter system is improved as the additional boost reactors are omitted by utilizing the leakage inductance of transformer.[1]
- Aiding effect of interleaved winding strategy is studied which helps integrating the low voltage PV with the ac grid.

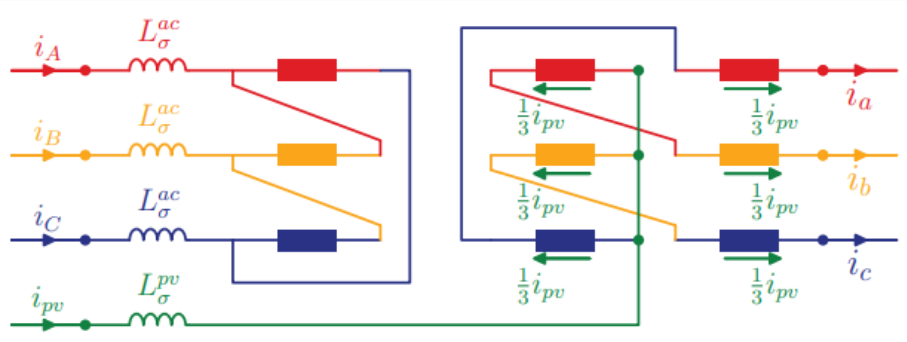

(a)

(b)

Fig. Proposed scheme in [1] depicts the integration of low voltage (LV) photovoltaic (PV) with ac grid using a single three-phase four-leg PWM rectifier.

[1] A. K. Das, A. Shetty and B. G. Fernandes, "Design Methodology of a Line-Frequency Zig-Zag Transformer to Utilize its Winding Leakage Inductances as Integrated Boost-Inductances in a Unified AC-DC System," ECCE 2018, pp. 3198-3205, doi: 10.1109/ECCE.2018.8557912.

Three Phase PWM Rectifier with Integrated Battery for Automotive Applications

- A novel topology of integrating the battery without the need of a seperate converter for the automotive generator is proposed, which reduces size and weight.[1]

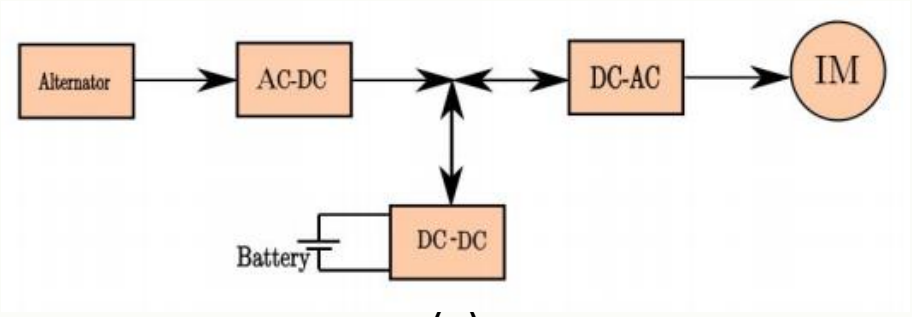

(a)

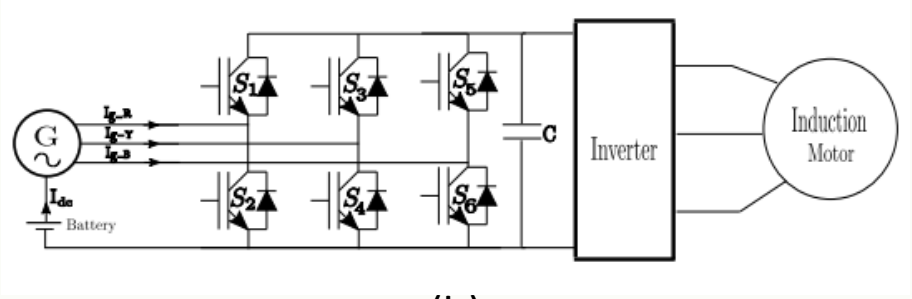

(b)

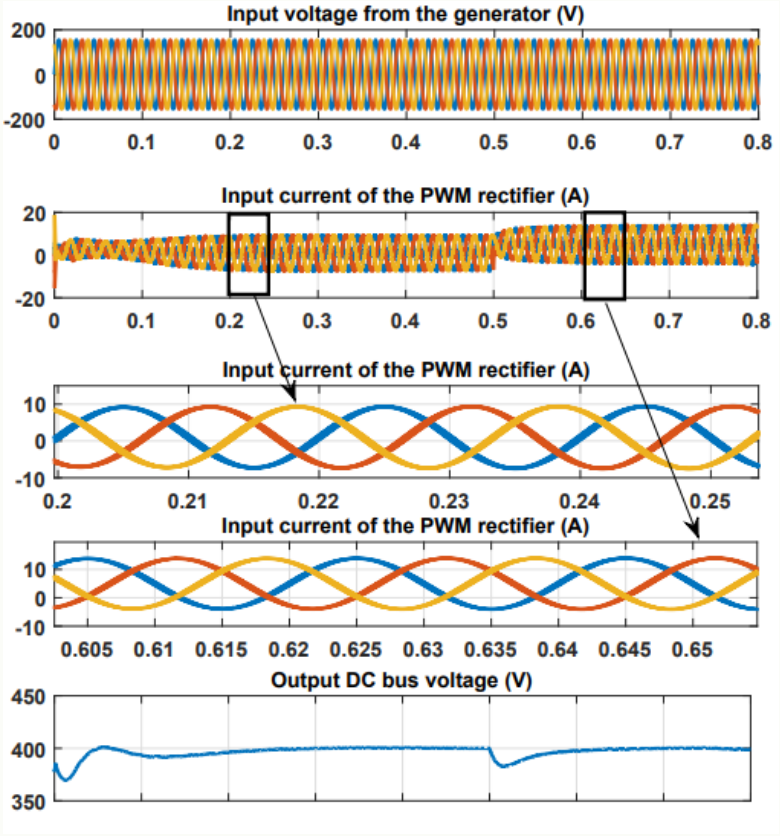

(c)

Fig. (a) Power train arrangement for a series HEV, (b) the proposed PWM rectifier topology, and (c) Performance during battery in discharging mode[1].

[1] A. Shetty, B. G. Fernandes, J. O. Ojo and J. A. Ferreira, "Three Phase PWM Rectifier with Integrated Battery for Automotive Applications," IAS 2018, pp. 1-6, doi: 10.1109/IAS.2018.8544681.

Bidirectional Z-Source Breaker for DC Micro-grid Protection

- Fast operating bidirectional solid state circuit breakers are developed which are suitable for protection of dc systems.[1],[2]

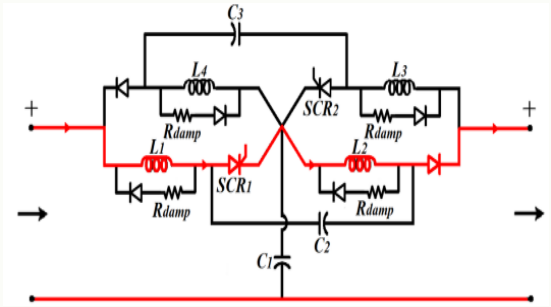

(a)

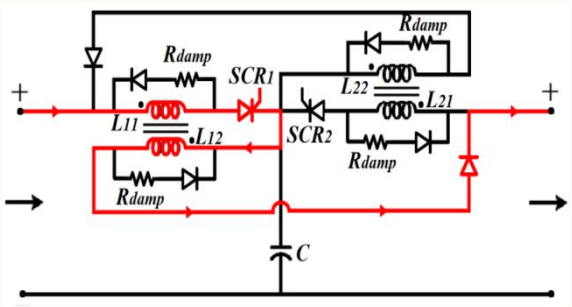

(b)

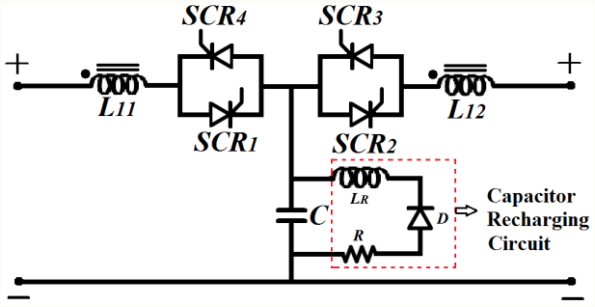

(c)

Fig. (a-c) Proposed topologies of the bidirectional Z-source breakers (Bi-ZSB)[1,2], and (d-e) the fabricated laboratory scale prototypes.

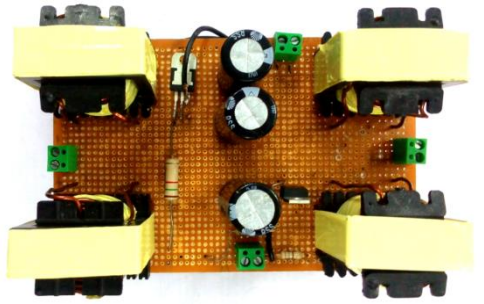

(d)

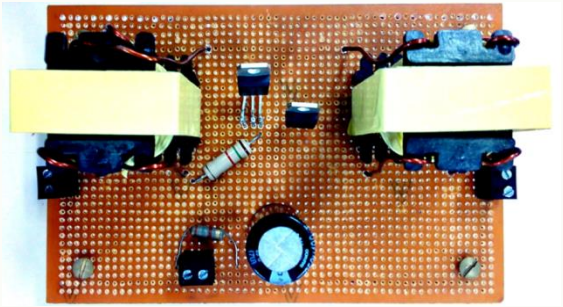

(e)

[1] S. G. Savaliya and B. G. Fernandes, "Analysis and Experimental Validation of Bidirectional Z-Source DC Circuit Breakers," in *IEEE Transactions on Industrial Electronics*, vol. 67, no. 6, pp. 4613-4622, June 2020.

[2] S. G. Savaliya and B. G. Fernandes, "Performance Evaluation of a Modified Bidirectional Z-Source Breaker," in *IEEE Transactions on Industrial Electronics*, vol. 68, no. 8, pp. 7137-7145, Aug. 2021.

Battery Management System (BMS) for Inhomogeneous Series-Connected Battery Strings

- Cell balancing, Accurate estimation of the State of Charge (SOC), and Online estimation of the State of Health (SoH).[1]

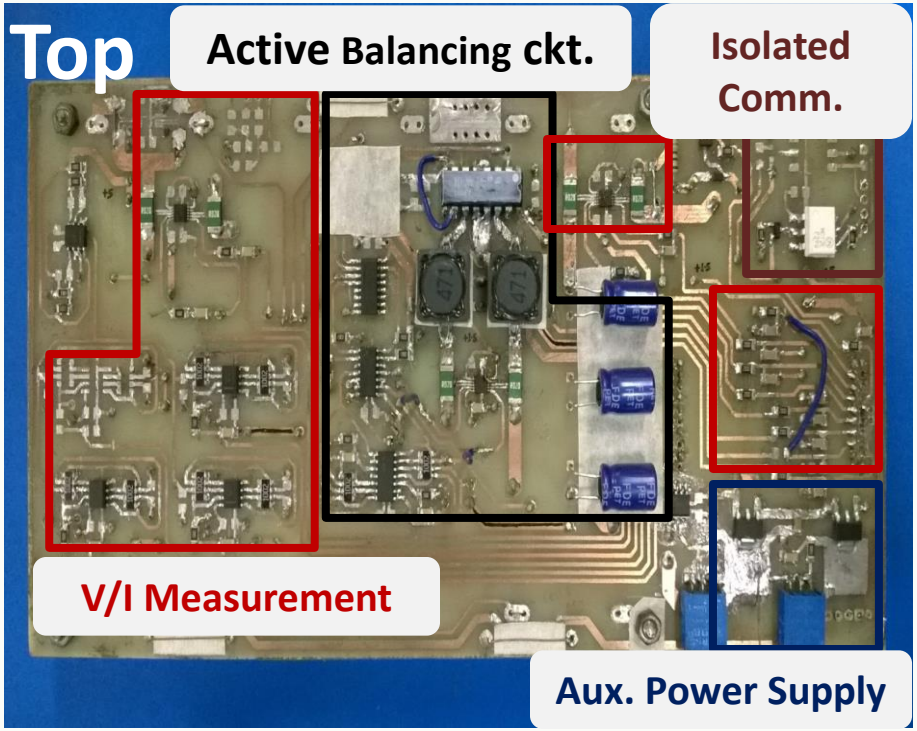

(a)

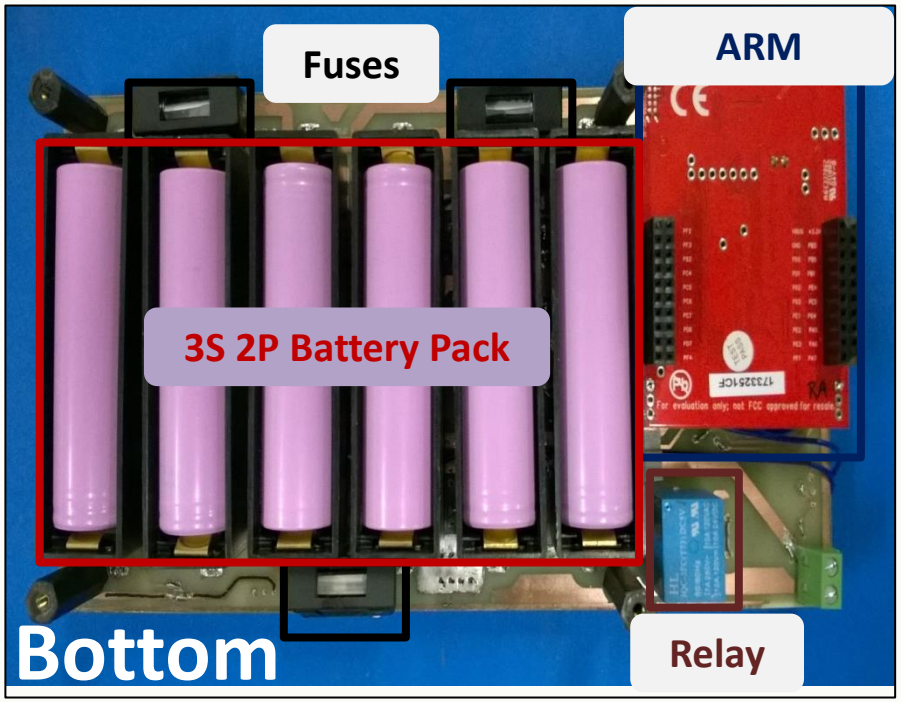

(b)

Fig. (a) Top and (b) Bottom views of the fabricated battery management system[1].

[1] R. Anand and B. G. Fernandes, "Simplified control strategy for an inhomogeneous series-connected battery string," ECCE 2019, pp. 5064-5071, doi: 10.1109/ECCE.2019.8913308.

An OVERVIEW of Research and Development Activities in GaN based PE Converter, Integration of RES in Microgrid, High-power Converter, and SST

PEPS, EE Department,

IIT Bombay

Modular Transformer-based Regenerative CMC Converter for drives with Multilevel operation at Input & Output

- A configuration of cascaded multicell converter (CMC) with single phase PWM rectifier-power cell is proposed in [1] for MV high-power regenerative drives.[1]

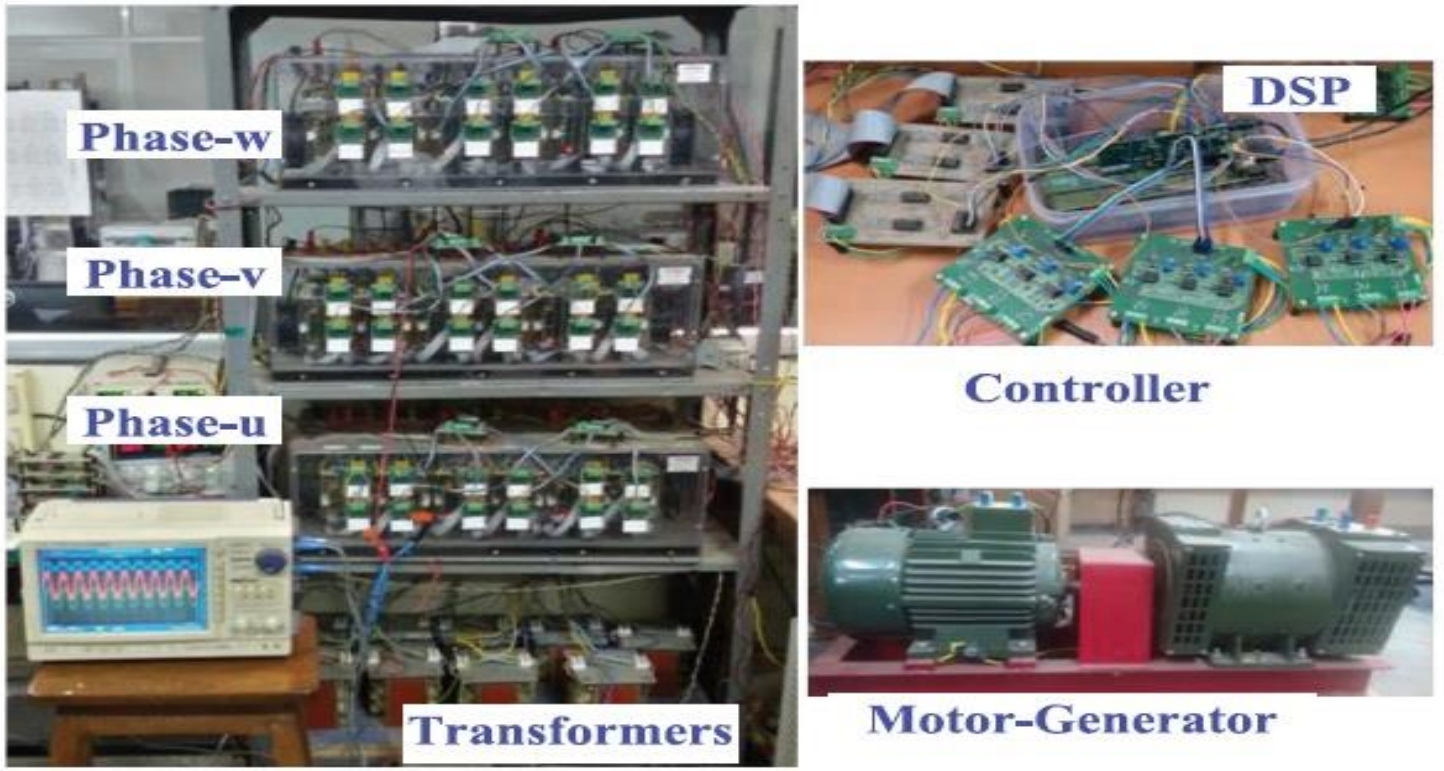

Fig. Experimental setup showing converter modules, DSP and motor-generator load[1].

[1] S. Sau, S. Karmakar and B. G. Fernandes, "Modular Transformer-Based Regenerative-Cascaded Multicell Converter for Drives With Multilevel Voltage Operation at Both Input and Output Sides," in *IEEE Transactions on Industrial Electronics*, vol. 65, no. 7, pp. 5313-5323, July 2018, doi: 10.1109/TIE.2017.2774733.

Modular Multilevel Converter Based Variable Speed Drive with Reduced Capacitor Ripple Voltage

- A new configuration of multi-pulse diode-bridge rectifier circuit is proposed.[1]
- It reduces the dc-bus voltage as speed reduces, is cost-effective, simple and robust solution for non-regenerative variable speed drive (VSD) application.

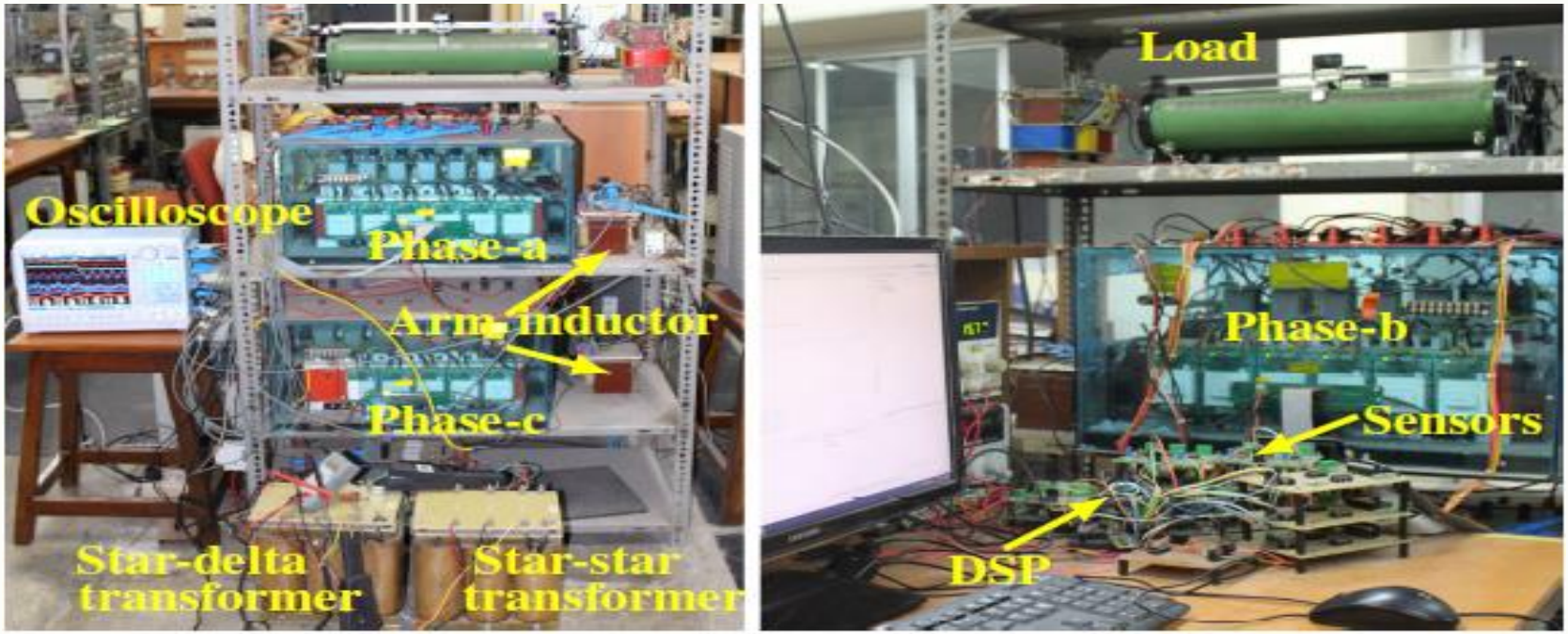

Fig. Experimental setup showing converter modules, DSP and motor-generator load[1].

[1] S. Sau and B. G. Fernandes, "Modular Multilevel Converter Based Variable Speed Drive With Reduced Capacitor Ripple Voltage," in *IEEE Transactions on Industrial Electronics*, vol. 66, no. 5, pp. 3412-3421, May 2019, doi: 10.1109/TIE.2018.2860542.

Elimination of Power Unbalance in Phases of CHB Converter for PV Integration

- Power unbalance in phases of CHB under unequal PV power generation is eliminated.[1]
- The DC-DC converter, connecting PV modules to the CHB, contains a high-frequency transformer with single input and three outputs; it tracks the MPP, provides isolation and eliminates the power unbalance in the phases of CHB.

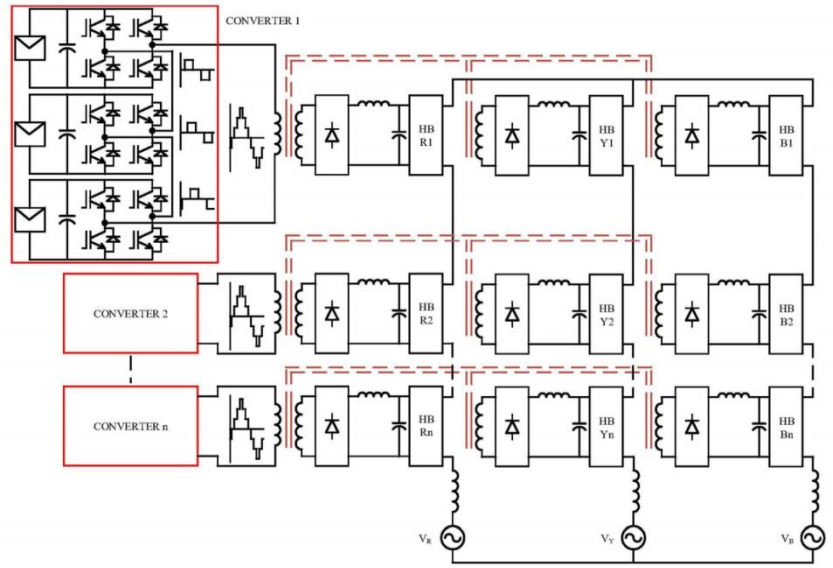

(a)

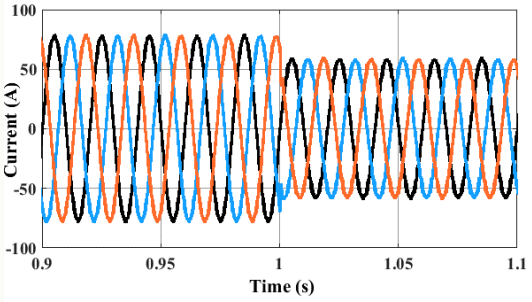

(b)

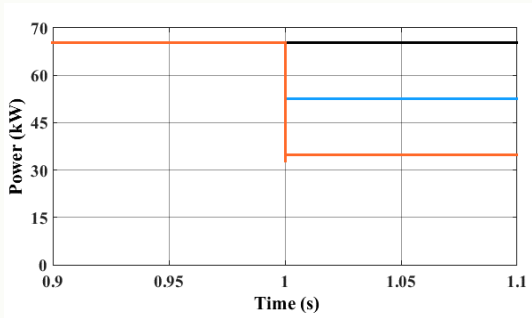

(c)

Fig. (a) Proposed converter, and Simulation results showing (b) Grid current and (c) PV generation[1].

---

[1] K. A. Ajith and B. G. Fernandes, "Elimination of Phase Unbalance in Cascaded Multilevel Converters for Large-Scale Photovoltaic Grid Integration," IAS 2019, pp. 1-5, doi: 10.1109/IAS.2019.8912358.

An OVERVIEW of Research and Development Activities in GaN based PE Converter, Integration of RES in Microgrid, High-power Converter, and SST

PEPS, EE Department,

IIT Bombay

A SST based Fast Charging Station for All Categories of Electric Vehicles

- Using SST topology, it integrates renewable energy sources (RES)such as PV and battery to each fast charging (FC) port.[1]
- It conforms to Level 3 dc fast charging of three different classes of electric vehicles (EV).

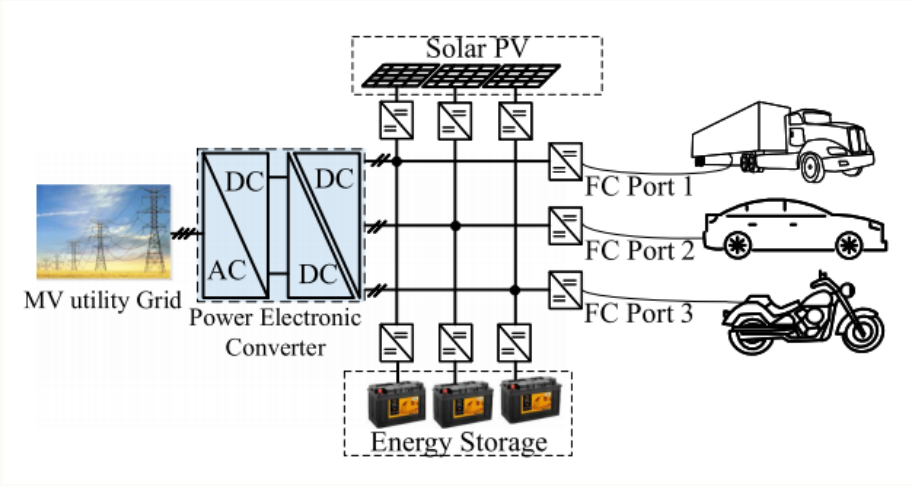

(a)

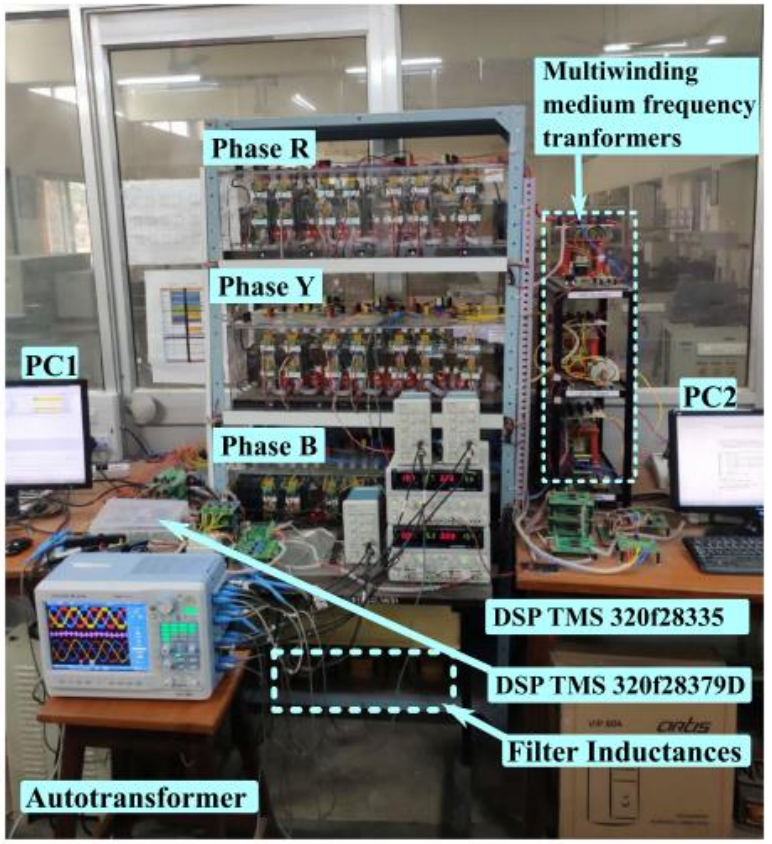

(b)

Fig. (a) Structure of the fast charging station, and (b) Laboratory scale hardware setup[1].

---

[1] A. C. Nair and B. G. Fernandes, "Solid-State Transformer Based Fast Charging Station for Various Categories of Electric Vehicles With Batteries of Vastly Different Ratings," in *IEEE Transactions on Industrial Electronics*, vol. 68, no. 11, pp. 10400-10411, Nov. 2021, doi: 10.1109/TIE.2020.3038091.

A Quad Active Bridge (QAB) based On-board Power Electronic Interface for an Electric Vehicle

- A QAB converter is proposed which acts as an on-board power electronic interface for an electric vehicle.[1]
- Power management scheme for the operation of the electric vehicle with QAB interface.
- Control strategy for effective power sharing between battery and ultra-capacitor (UC).
- Simulation studies and Experimental results to verify the effectiveness of the HESS control in sharing the power between UC and battery.

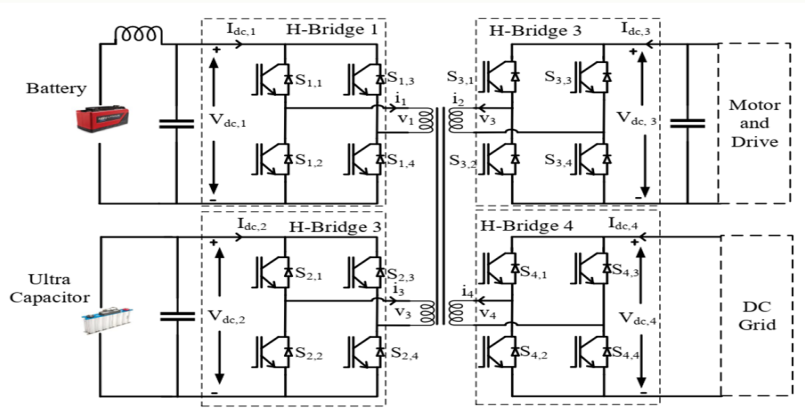

(a)

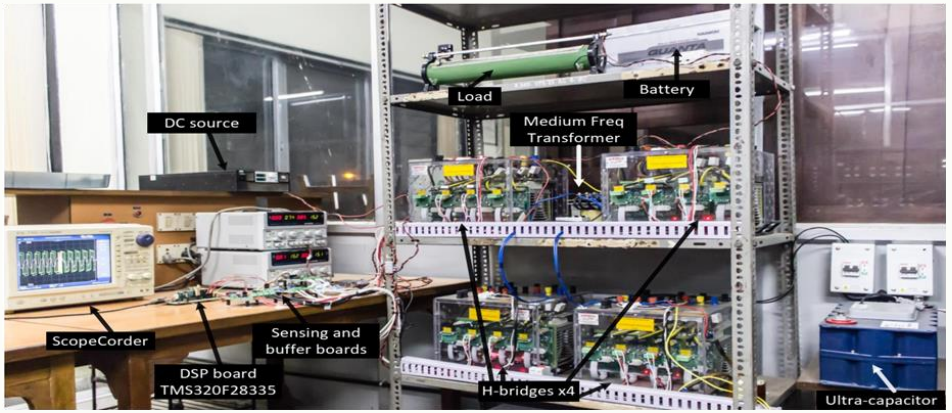

(b)

Fig. (a) Proposed QAB converter allows power transfer from HESS to drive and charging from a DC grid, and (b) Laboratory scale hardware setup[1].

---

[1] A. C. Nair, Vishal M.J. and B.G. Fernandes "A Quad Active Bridge based On-board Power Electronic Interface for an Electric Vehicle," *2018 IEEE Energy Conversion Congress and Exposition (ECCE)*, Portland, Oregon, 2018.

Minimum RMS Current Operation of Isolated DAB DC-DC Converter Employing DPS Control

- Universal trajectory is derived for dual phase-shift (DPS) control of a DAB converter to minimize the reactive power flow and thereby improve the efficiency.[1]

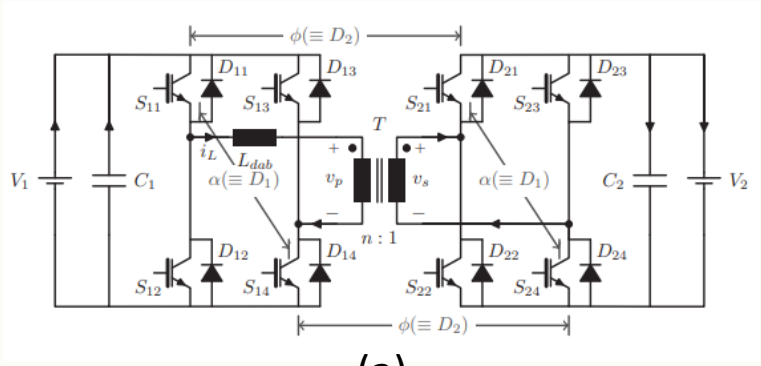

(a)

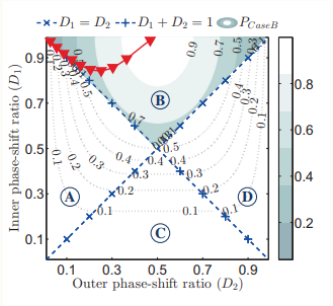

(b)

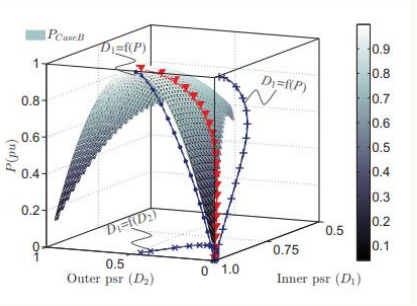

(c)

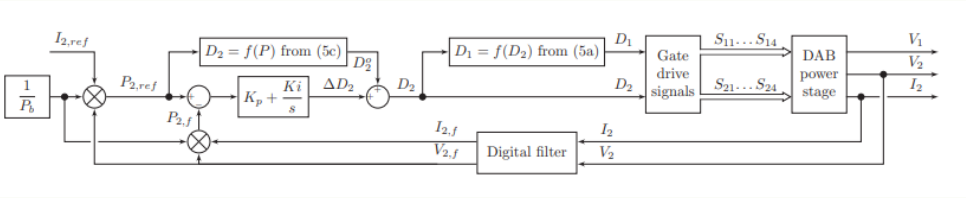

(d)

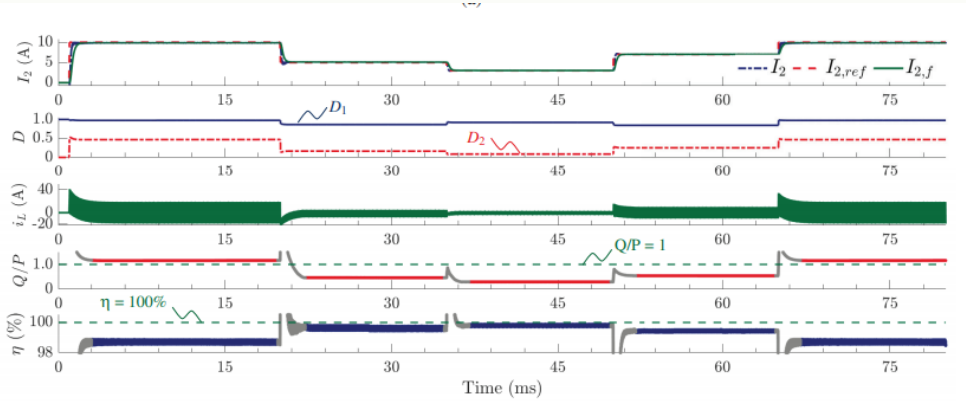

(e)

Fig. (a) Schematic of a DAB converter, (b-c) The proposed minimum rms current trajectory, and (d-e) The closed-loop control and simulation results[1].

[1] A. K. Das and B. G. Fernandes, "Fully ZVS, Minimum RMS Current Operation of Isolated Dual Active Bridge DC-DC Converter Employing Dual Phase-Shift Control," EPE 2019, pp. P.1-P.10, doi: 10.23919/EPE.2019.8914975.

Resonance Frequency Estimation Using an Equivalent π-model of 2-winding HF Transformer

- Natural resonance frequencies of a high-frequency two-winding transformer are estimated analytically using an equivalent pi-model representation.[1]

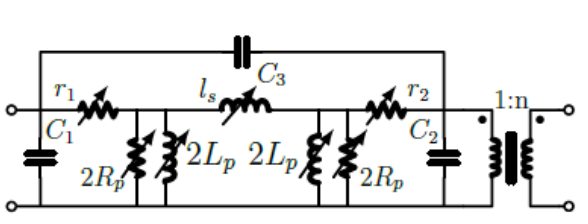

(a)

$$Z'_{AB} = \frac{1}{C_3} \frac{(a_3 s^3 + a_2 s^2 + a_1 s + a_0)}{(b_4 s^4 + b_3 s^3 + b_2 s^2 + b_1 s + b_0)}$$

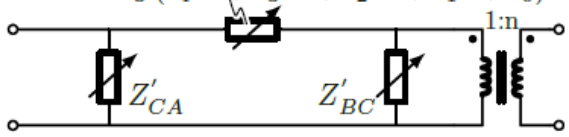

(b)

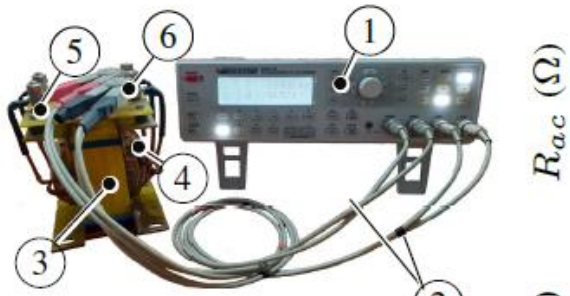

1 – LCR meter (HM8118)
2 – Kelvin test leads
3, 4 – EE core and winding assembly
5 – Primary (HV) winding terminals
6 – Secondary (LV) winding terminals

(c)

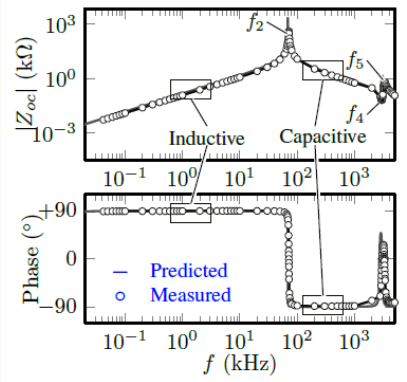

(d)

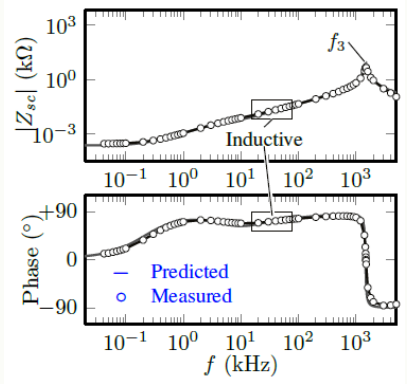

(e)

Fig. (a) Capacitive pi-model of a high-frequency two-winding transformer and (b) its equivalent transfer function based representation, (c) Lumped circuit measurement using a LCR meter, and (d-e) Estimated and measured resonance frequencies.

---

[1] A. K. Das and B. G. Fernandes, "Synthesis of an Equivalent π-model of Two-winding Transformer and Resonance Frequency Estimation Using Lumped Circuit Parameters," ECCE 2019, pp. 3025-3032.

99.55% Efficient, 10 kW, 0.5/5 kV, 1 kHz Transformer Optimized Using Gradient Method

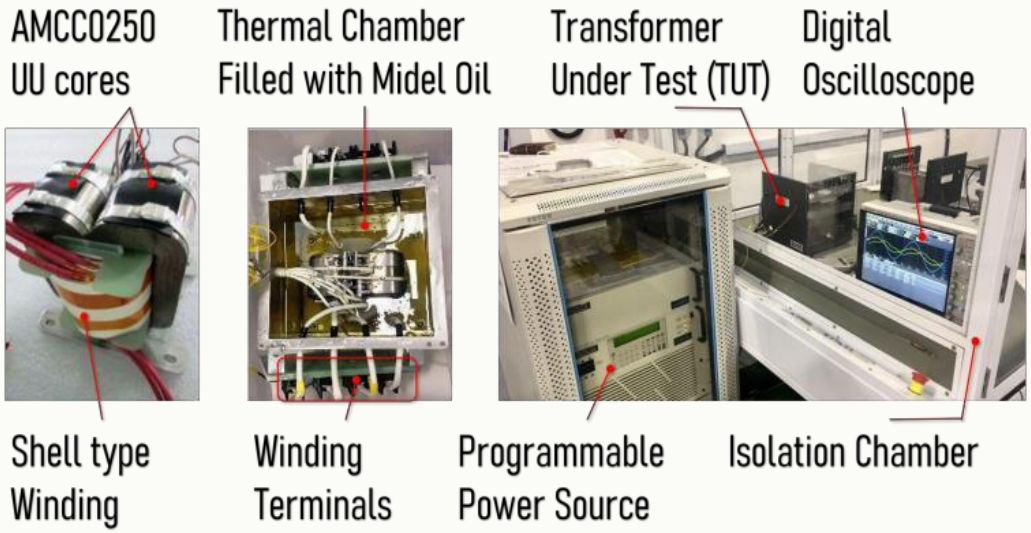

Power density (w/o tank) is 19.79 kW/dm^3, Maximum ΔT_j < 33 °C.

A. K. Das et. al., "Multi-variable optimization methodology for medium-frequency high-power transformer design employing steepest descent method," 2018 IEEE Applied Power Electronics Conference and Exposition (APEC), SanAntonio, TX, USA, 2018, pp. 1786-1793.

Hybrid AC DC Single stage Multifunctional PWM Converter for Integrating LV PV with 3 φ AC

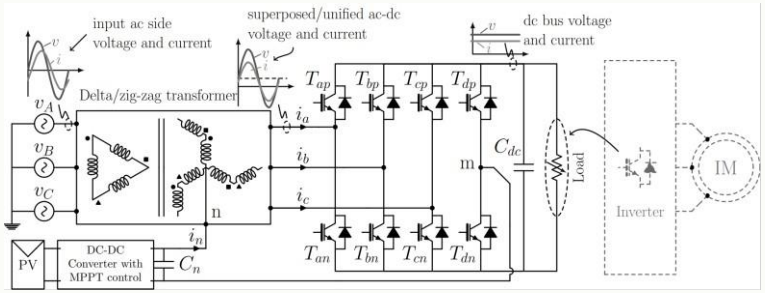

Low voltage solar PV is integrated with three-phase ac grid using a delta/zigzag transformer and four-legged PWM converter.

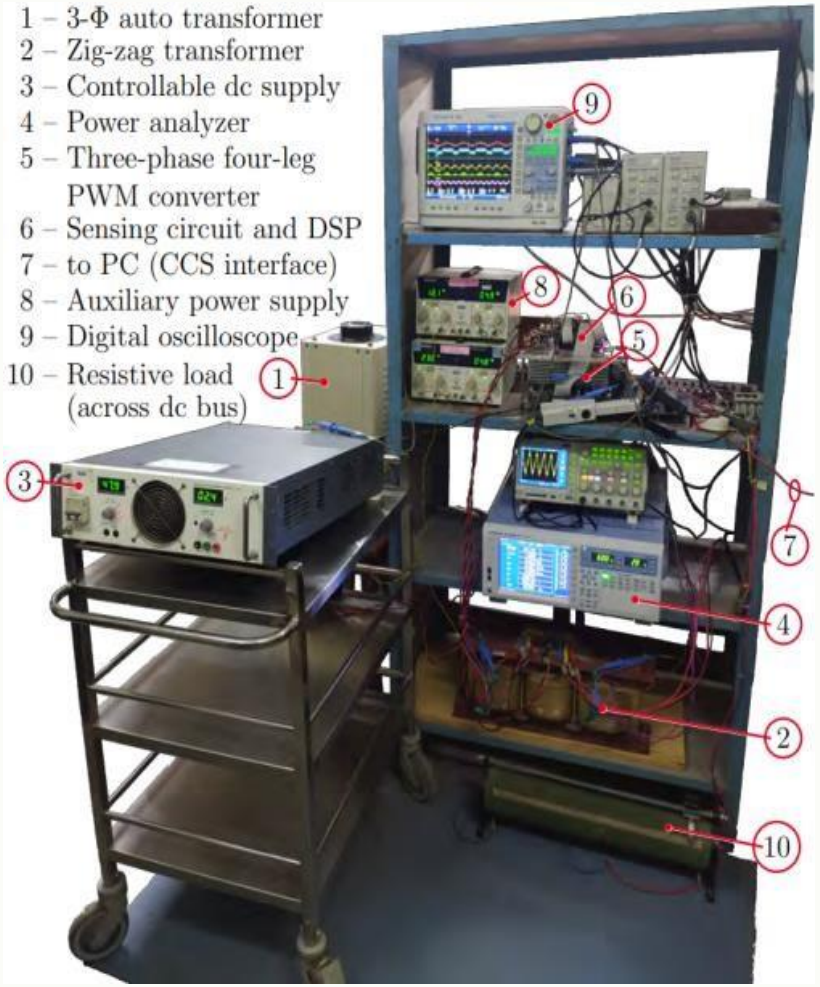

V. Chitranshetal., "Evaluation of Multi-frequency Power Electronic Converters: Concept, Architectures, and Realization," in IEEE Journal of Emerging and Selected Topics in Power Electronics, vol. 9, no. 3, pp. 3582-3597, June2021.

Design, Fabrication and Validation of 1.2 kW, 0.24/2.1kV, 20 kHz Foil Winding Transformers

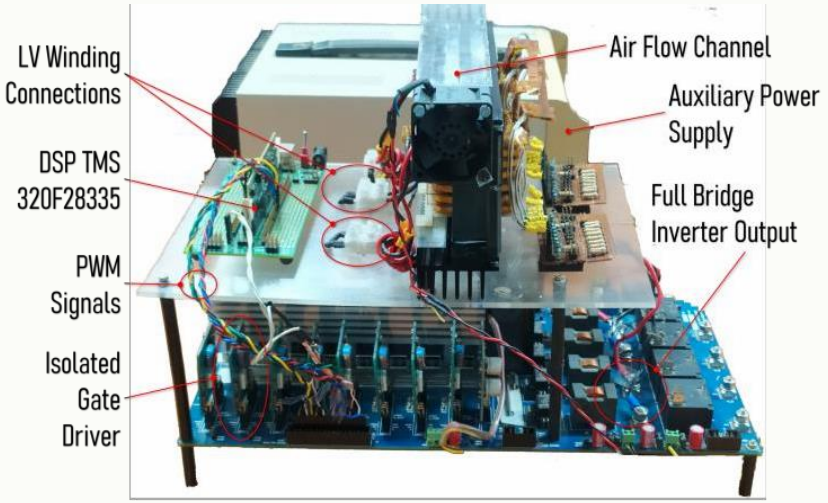

Bus Bar Connection between the High Voltage (HV) Terminals of the Transformers Prototypes

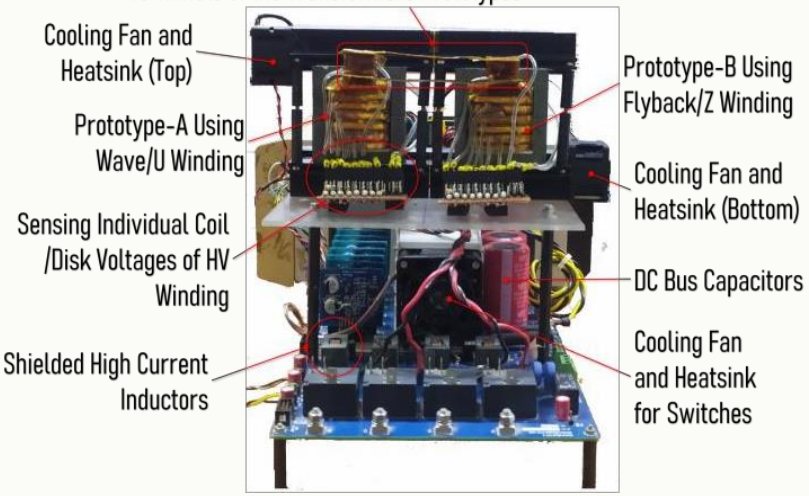

- Two foil winding transformers of similar ratings but different winding schemes (wave and flyback) are shown connected in back-to-back fashion (Sumpner's test) along with the converter.

Thank you